

Solid-State Transformer and Hybrid Transformer with Integrated Energy Storage in Active Distribution Grids: Technical and Economic Comparison, Dispatch, and Control

Liran Zheng, *Member, IEEE*, Aniruddh Marellapudi, *Student Member, IEEE*, Vikram Roy Chowdhury, *Member, IEEE*, Nishant Bilakanti, *Student Member, IEEE*, Rajendra Prasad Kandula, *Member, IEEE*, Maryam Saedifard, *Fellow, IEEE*, Santiago Grijalva, *Senior Member, IEEE*, and Deepak Divan, *Life Fellow, IEEE*

Abstract—Solid-state transformer (SST) and hybrid transformer (HT) are promising alternatives to the line-frequency transformer (LFT) in smart grids. The SST features medium-frequency isolation, full controllability for voltage regulation, reactive power compensation, and the capability of battery energy storage system (BESS) integration with multiport configuration. The HT has a partially-rated converter for fractional controllability and can integrate a small BESS. Fast grid-edge voltage fluctuations from increased solar photovoltaic (PV) and electric vehicle (EV) penetration are difficult to manage for mechanical load tap changers. Hence, along with the trend towards more BESS in the grid, the controllability and the storage integration capability of the SST and HT are of strong interest. However, a review of literature shows existing SST and HT research is mostly at converter level, while system-level assessments are scarce. Assessing technical and economic impacts is critical to understanding the benefits and role of the SST and HT to guide future research, which is presented for the first time in this article. Experimental results from medium-voltage (MV) SST and MV HT prototypes are shown to confirm equipment-level feasibility, where the voltage controllability waveforms of a MV HT prototype are reported for the first time. Comparative simulations are performed on a modified IEEE 34-bus system. A grid-model-less decentralized grid-edge voltage control method and a day-ahead BESS dispatch method are proposed for the SST and HT. The simulations show that the SST and HT with integrated storage can host more PV, achieve peak shaving, mitigate voltage fluctuation and reverse power flow, and support energy arbitrage for operational cost reduction, as compared to the LFT. Moreover, comprehensive analyses of net present value (NPV) and internal rate of return (IRR) are performed under different installed PV capacities, HT's partial converter ratings, and BESS capacities. Sensitivities to future cost reductions of the PV and BESS are studied. Although the NPV and IRR are currently negative, 60% capital cost reduction or 150% revenue increase will make the SST and HT economically viable in the use case studied.

Index Terms—Distributed renewable energy resource (DER), solid-state transformer (SST), hybrid transformer (HT), power electronic transformer (PET), medium-frequency transformer (MFT), active distribution network (ADN), load tap changer (LTC), electric vehicle (EV).

I. INTRODUCTION

THERE is a growing trend towards increased penetration of distributed energy resources (DERs) in active distribution networks (ADN) [1]-[3]. In addition, electric vehicles (EVs) and EV charging infrastructure are booming [4]-[5]. The integration of these intermittent resources, however, creates problems in the grid, one of the most severe being the voltage rise at the end of the feeder due to active power injection from photovoltaic (PV) power generation [1]-[3]. Increased installations of EV chargers and vehicle-to-grid (V2G) technologies promising bidirectional power flow can exacerbate this problem [4]-[5]. To safely utilize and realize the benefits of DERs, the voltage fluctuation should be kept within safe limits [1]-[3]. However, traditional voltage regulation devices including load tap changers (LTCs) and switched capacitor banks are slow and can only operate a few times each day during their lifetime. Hence, they cannot satisfy the voltage regulation requirements with fluctuating PV sources or EV chargers in ADNs [1]-[3], [6]. Another growing trend in the distribution grids is the proliferation of energy storage, which can be used for peak shaving, volt/var support, and energy arbitrage to reduce total electricity cost [7]-[9].

The solid-state transformer (SST), also known as power electronic transformer (PET), is envisioned to replace the line-frequency transformer (LFT) with a medium-frequency isolated power converter for controllability and storage integration to address the aforementioned issues in distribution grids [10]-[14]. Recent advances in medium-voltage (MV) SiC devices have led to enormous interests in SSTs and PETs [15]-[16]. Significant progress has been made in converter protection [17]-[19], topologies such as single-stage current-source circuits [14], [20]-[21], resonant converter circuits [22], dual-active-bridge circuits [23]-[25], and matrix-type circuits [26]-[27], converter controls [28]-[35], applications [36]-[41] in PV, microgrids, etc., and auxiliary components [42]. Importantly, MV experimental prototypes [14], [20]-[24] have shown high efficiency of about 97% for AC-AC conversion,

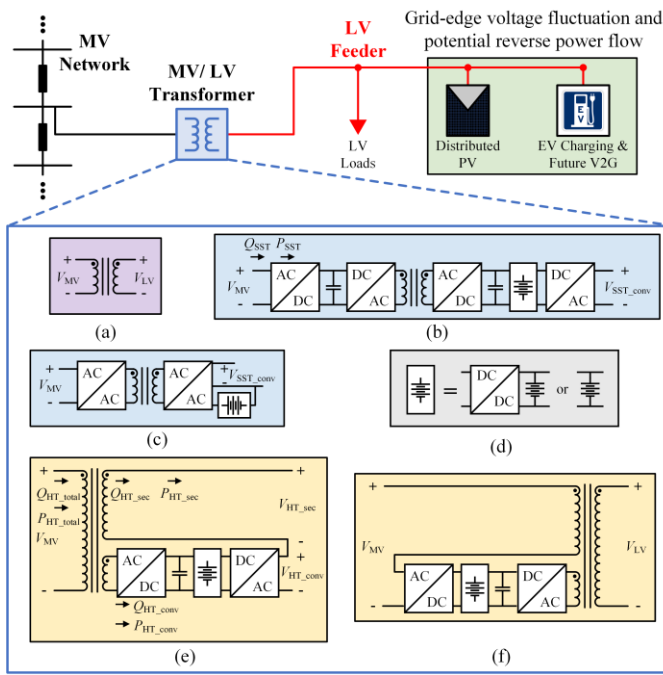


Fig. 1. Solid-state transformer (SST) and the hybrid transformer (HT) with integrated storage in active distribution grids. (a) Line-frequency transformer. (b)-(c) SST. Both the three-stage SST in (b) and the single-stage current-source SST [14] in (c) can realize controllability and storage integration. (d) Energy storage. (e)-(f) HT. The converter in the HT can be installed either on (e) LV side or (f) MV side of the transformer.

and industrial trials of the SST have been reported in [43]. Besides the aforementioned equipment-level SST research, some system-level SST research has been performed. A voltage control and dispatch method for SST is proposed in [44]. Energy management methods for SST-fed DC microgrids [45], converter interaction and stability [46]-[47] are also studied. The modeling and simulation of SST for power system analysis are discussed in [48]-[49]. However, the impacts and economics of the SST from the controllability and the integrated battery energy storage system (BESS) to address fluctuating DERs in a distribution grid have not been addressed. Furthermore, system-level impact and economic comparisons for the hybrid transformer (HT) and the LFT are needed.

The HT is a LFT that incorporates a partially-rated power converter for $\sim 5\%$ - 20% controllability. With fractionally-rated power electronics, the HT is less expensive and more efficient than the SST and is better targeted for near-term applications [2], [50]. Research progress has been made on protection concepts [51] and hardware design [52]. The HT can also be used as a voltage sag corrector [53]-[54]. The HT prototypes based on back-to-back voltage-source converters [55] and direct AC-AC converters [56]-[57] for power flow control have been built and tested [58].

The existing research on the HT is mainly focused on converter-level analysis, though a comprehensive qualitative view of the HT's functionality in distribution grids is presented in [50]. A quantitative assessment of the HT's system-level

impact is missing in the literature. Moreover, the proliferation of PV and storage needs to be considered to better understand the role of the HT in emerging distribution grids. Therefore, the first contribution of this article is on the quantitative assessment of the HT with an integrated storage. To the authors' best knowledge, the HT with integrated storage in Fig. 1 and the impacts on the distribution grid, i.e., the benefits from the controllability and the storage with dispatch and control methods have not been studied in the literature. For the SST, the authors believe that it is very important to discuss the challenges and applicability of the SST. The grid-connected applications of the SST is presented qualitatively and conceptually in [59]. Quantitative assessment of technical and economic aspects in the distribution grid application is covered in this article, which is the second contribution of the article. In other words, comparative quantitative impact assessment and economic analysis on the controllability of the SST and the HT to increase PV penetration and integrate storage as compared to a LFT have not yet been studied in the literature, to the authors' best knowledge. Generally, with falling costs of MV SiC devices, increased needs for controllability in the distribution grid [1]-[2], and more efficient, robust, and reliable converters, higher penetration of power electronics is a general trend [6], [60]-[61]. It is critical to understand the system-level technical and economic benefits from the power electronic equipment such as the HT and the SST and the differences of these impacts from the different controllability of the HT and the SST.

This article is an attempt to address the aforementioned research gap and to compare the performance of the SST with integrated storage, the HT with integrated storage, and the LFT in the distribution grid from both technical and economic perspectives. Moreover, to realize and compare the controllability and the storage integration capability in the grid, appropriate dispatch and control methods are required. A grid-edge voltage control method without the need of a grid model, and a day-ahead BESS dispatch method are presented for the HT and the SST with integrated storage.

The rest of this article is organized as follows. Different aspects of the SST, the HT, and the LFT in the distribution grid application are introduced in Section II. Section III presents the modified IEEE 34-bus testing network and installed SST and HT configurations. The control and the dispatch method are covered in Section IV. Section V describes equipment-level results of MV SST and HT prototypes. Then, the system-level technical and economic impacts are discussed in Section VI and Section VII, respectively. Section VIII concludes the article.

II. SOLID-STATE, HYBRID, AND LINE-FREQUENCY TRANSFORMERS IN ACTIVE DISTRIBUTION GRIDS

Different aspects of the SST, the HT, and the LFT in the distribution grid application are introduced. The SST has a fully-rated power converter with a medium-frequency transformer (MFT). Therefore, the SST can achieve voltage control, reactive power injection, harmonic filtering, and energy storage integration up to the 100% voltage and power

TABLE I
Solid-state transformer (SST), hybrid transformer (HT) and line-frequency transformer (LFT) in distribution grids

	SST	HT	LFT
Controllability	100% voltage, power	5%-20% voltage, power	No
Functionality	Integrated storage, system-level support from storage, voltage control, var injection, and active filtering up to the voltage/power controllability rating		No
Efficiency	97%	98.6%-98.9%	99%
Lifetime	20 yrs	20 yrs converter, 30-40 yrs transformer	30-40 yrs
Reliability	Depends on the modularity of the design	High, with fail-normal switch	High
Protection	Difficult, sensitive to surge	Medium, with fail-normal switch	Easy
Cost	High, but much lower than PV/storage	Low	Lower
Size	Small	Large	Large
Manufacturability	Difficult	Medium	Easy

rating of the power converter. The system-level support from the integrated energy storage can also be provided. The HT with a partially-rated converter can provide similar services but only up to its fractional rating of the converter. Here, the fractional rating is normally between 5% and 20%, depending on the specific design and applications. The LFT does not have any controllability without a power converter or a LTC. Importantly, to realize the controllability and the storage integration advantages from the topology of the SST and the HT in active distribution grids, appropriate dispatch and control methods are required.

The LFT has the highest efficiency of 99%. The SST has all the power flowing through electronic conversion stages. The estimated efficiency is around 97% [20]. For the HT, only 5%-20% of the power is processed through a rectifier and an inverter, and the rest only flows through the transformer. With a 99% efficient rectifier and a 99% efficient inverter, the efficiency of the HT is 98.6%-98.9% which is close to a LFT. The lifetime of power converters can be as long as 20 years with a reliability-oriented design, while the transformer can last 30-40 years. Thus, the SST has the shortest lifetime. For the HT, considering that the fail-normal switch [55]-[58] can bypass the converter under failures for the operation at least like a LFT, the shorter lifetime of the converter is of less concern. Regarding reliability, the LFT and the HT with a fail-normal switch are robust. The SST's reliability highly depends on the architecture. A modular design with redundant modules is preferred for high reliability [20]-[21].

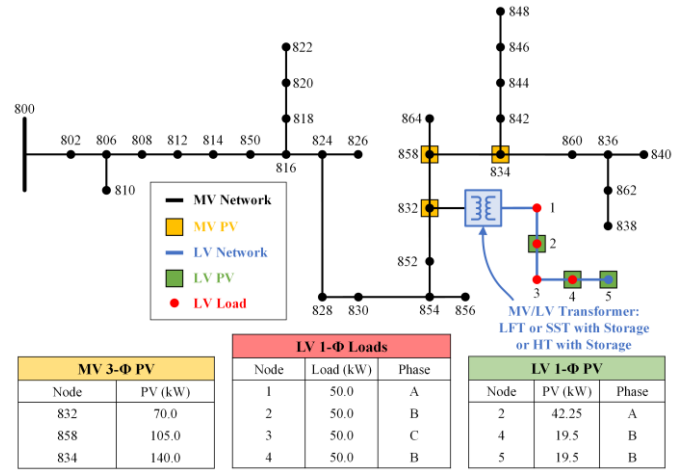


Fig. 2. Modified IEEE 34-bus system [62] with the conventional line-frequency transformer (LFT) at node 832 replaced by either a solid-state transformer (SST) or a hybrid transformer (HT) in test cases. The SST or the HT is coupled to a modified LV feeder benchmark [63]. Single-phase and three-phase PVs are installed on the LV grid and the MV grid.

The protection of the SST is a key challenge as semiconductors are sensitive to overvoltage or overcurrent. Especially, protection schemes for lightning surge and basic insulation level are required [17]. Fault current sourcing for compatibility with legacy protection systems is another issue, where devices with overrated current rating are potentially needed. For the HT, with the fail-normal switch to bypass the converter, the fault current can be sourced from the transformer directly, which makes the protection design easier than the SST [51], [55]-[58]. The protection design of the LFT is relatively mature and reliable.

The cost of the SST is much higher than the LFT and the HT. For example, according to the authors' 7.2 kV 50 kVA MV SST and HT prototypes in Section V, the SST cost is estimated to be 86.2 \$/kVA, i.e., 3.4 times of a LFT, when the HT has 31.7 \$/kVA estimated cost. However, note that the per kVA cost of the SST is still much lower than the PV or the BESS as will be detailed in Section VII. Regarding volume, the SST enjoys a power density of 2.7 W/in³ which is 22% higher than the LFT of 2.2 W/in³, as measured from the authors' prototypes in Section V. The HT's size is very similar to the LFT, e.g., only 5%-10% larger due to the fractionally rated converter. As to manufacturability, the SST requires significant realization and integration efforts, especially for modular design with more than one set of peripherals including sensors, gate drivers, etc. The additional efforts of HT compared to the LFT include a tertiary winding or additional transformer taps and a partially-rated power converter. The passive LFT can be manufactured much easier than the SST and the HT.

Overall, the SST and the HT have better performance metrics including controllability and functionality but higher cost, as summarized in Table I. The next question is whether the additional controllability and functionality can justify the higher cost. To evaluate the technical benefits, the test network will be discussed in the next section. The dispatch and control methods for the SST and the HT are necessary for the

controllability and functionality, which will be covered in Section IV.

III. TEST NETWORK AND INSTALLED SOLID-STATE TRANSFORMER AND HYBRID TRANSFORMER CONFIGURATIONS

The IEEE 34-bus system with PQ loads and constant impedance loads in [62] is modified and used as shown in Fig. 2. The conventional MV/LV LFT at node 832 in the original IEEE 34-bus system is replaced with either a SST with integrated storage or a HT with integrated storage in Fig. 1 to study the impacts. The LV-side of the SST or the HT supplies the modified LV feeder reference network [63], which is converted to the voltage level of US 120 V/240 V split-phase systems. The LV feeder lengths between consecutive nodes (beginning with node 1) are 100 m, 150 m, 200 m, and 200 m, respectively. The locations and sizes of the loads on the LV feeder and the locations of the PV systems on the MV grid and the LV feeder are fixed in all test cases as shown in Fig. 2. The PV sizes in Fig. 2 correspond to the case of the SST, while the HT and the LFT host less PV as will be shown in Section VI. The voltage fluctuation from the PV can lead to severe and unacceptable mechanical wear of the LTCs [1]-[3], [6]. Hence, the settings of the LTCs are fixed at their default values in the simulations.

As this article aims to understand the system-level impacts at the line frequency rather than the switching frequency, the switching ripple is neglected [64] and the AC/DC and DC/AC stages in the HT and the SST in Fig. 1 are modeled as current sources or equivalently active and reactive power drawn from the MV grid through the transformer tertiary winding (in the HT case) or directly (in the SST case), and voltage sources which supply the LV feeder. In the HT of Fig. 1, the DC/AC converter can produce a voltage V_{HT_conv} on top of the transformer secondary voltage V_{HT_sec} . The sum of the two voltages produces the controlled feeder-head voltage V_{HT_fh} in (1). In the SST of Fig. 1, the output voltage V_{SST_conv} of the DC/AC converter produces the controlled feeder-head voltage V_{SST_fh} in (2).

$$V_{HT_fh} = V_{HT_conv} + V_{HT_sec} \quad (1)$$

$$V_{SST_fh} = V_{SST_conv} \quad (2)$$

On the other hand, the AC/DC converter of the HT, which is coupled to the transformer tertiary winding, can inject reactive power Q_{HT_conv} , into the MV grid. The total reactive power drawn from the MV grid Q_{HT_total} in (3) is the sum of Q_{HT_sec} from the LV feeder and Q_{HT_conv} . The active power injection P_{HT_total} is determined by the load power P_{load} and the PV power P_{pv} on the LV feeder and the DC-link BESS power P_{HT_bat} in (4). Similarly, in (5), the AC/DC converter of the SST can perform the reactive power injection Q_{SST_total} into the MV grid, which is used to control the MV-side voltage via volt/var support. The active power injection P_{SST_total} in (6) is also determined by the LV-feeder net load and the BESS power

P_{SST_bat} . The major differences between the SST and the HT include the voltage/power rating and controllability of the power converter, and the power rating of the integrated BESS (1 pu for the SST and 0.05-0.2 pu for the HT).

$$Q_{HT_total} = Q_{HT_conv} + Q_{HT_sec} \quad (3)$$

$$P_{HT_total} = P_{HT_conv} + P_{HT_sec} = P_{load} - P_{pv} + P_{HT_bat} \quad (4)$$

$$Q_{SST_total} = Q_{SST_conv} \quad (5)$$

$$P_{SST_total} = P_{SST_conv} = P_{load} - P_{pv} + P_{SST_bat} \quad (6)$$

The references for the LV feeder-head (node 1) voltages V_{HT_fh} and V_{SST_fh} , the reactive power injection Q_{HT_conv} and Q_{SST_conv} into the MV grid, and the dispatched battery power P_{HT_bat} and P_{SST_bat} are derived by the control and dispatch methods in the following section.

IV. PROPOSED DAY-AHEAD DISPATCH OF THE BESS AND CONTROL METHODS FOR VOLTAGE FLUCTUATION MITIGATION

A. Day-Ahead Dispatch for the BESS

The SST and the HT have the capability of integrating the BESS with only an additional DC/DC converter as the interface or without any additional power converter. In particular, to realize the storage-integration capability, an appropriate dispatch and control method is required. In this article, peak shaving, energy arbitrage for electricity cost reduction, and upstream reverse-power-flow mitigation are studied. In other words, this article covers most of the benefits of the BESS in the distribution system in [7]-[9], with the voltage regulation from the SST or the HT.

Under high-penetration PV generation, reverse power flow can occur, interfering with the overcurrent protection relay [1]. The reverse power flow also impacts the settings of the LTCs [1]. Moreover, net metering policies which pay prosumers for back-feeding power are controversial in some regions and cause cost recovery issues for the distribution system operator [65].

Therefore, the following battery dispatch problem is formulated to achieve peak shaving, energy arbitrage, and reverse power flow mitigation. The cost function for day-ahead dispatch includes time-of-use electricity charge, demand charge, and degradation cost of the BESS as given in (7).

$$\text{Min } f = \sum_{t=1}^N P_{total}^t LMP^t T + P_{total,peak}^t C_{demand} + \sum_{t=1}^N |P_{bat}^t| C_{bat} T \quad (7)$$

where LMP^t is the locational marginal price every hour ($T=1$ hr) throughout a day which is estimated one day ahead and P_{total}^t is the total active power drawn from the MV grid. The electricity charge is calculated every hour and summed throughout a day ($N=24$), a month ($N=720$), or a year ($N=8760$). $P_{total,peak}^t C_{demand}$ is the demand charge paid once per billing cycle (a month), where $P_{total,peak}^t$ is the peak hourly power usage of P_{total}^t in the billing cycle and C_{demand} is the demand charge. Therefore, when the cost function is minimized, the demand-charge term naturally tries to smooth out the power usage profile and penalizes huge peak power. C_{bat} is the battery

degradation cost at 0.027 \$/kWh, assuming a battery cost of 190 \$/kWh and a lifecycle of 3500 cycles [66]. P_{bat}^t is the hourly battery power usage. The optimization problem in (7) can be converted and solved in the form of linear programming [67].

The total active power drawn from the MV grid P_{total}^t in (7) is calculated by (8). P_{total}^t , being a general symbol, would be $P_{\text{SST_total}}^t$ for the SST case and $P_{\text{HT_total}}^t$ for the HT case. In other words, (8) has the same meaning as (4) or (6). To avoid reverse power flow from the LV feeder into the MV grid, (9) is enforced as a constraint of the optimization problem.

$$P_{\text{total}}^t = P_{\text{load}}^t - P_{\text{pv}}^t + P_{\text{bat}}^t \quad (8)$$

$$P_{\text{total}}^t > 0 \quad (9)$$

The BESS can be charged to increase its state of charge (SoC) as in (10a) or discharged as in (10b). The efficiency η_{bat} of the BESS is assumed to be 95%, yielding a ~90% round-trip efficiency [66]. Equation (11) ensures that the initial SoC of the BESS equals the final SoC in each day. In (12), the BESS should not operate above 80% SoC ($\text{SoC}_{\text{bat,max}}$) or below 20% SoC ($\text{SoC}_{\text{bat,min}}$) to mitigate degradation [66]. The constraints of peak BESS power within the rated power ($P_{\text{bat,rated}}$) are shown in (13). While (4), (6), and (8) are similar and the same optimization method is used, the power and energy sizings are different for the SST and the HT.

When $P_{\text{bat}}^t > 0$, the battery is charged according to,

$$\text{SoC}_{\text{bat}}^t = \text{SoC}_{\text{bat}}^{t-1} + \eta_{\text{bat}} P_{\text{bat}}^t T / \text{Cap}_{\text{bat}} \quad (10a)$$

When $P_{\text{bat}}^t < 0$, the battery is discharged according to,

$$\text{SoC}_{\text{bat}}^t = \text{SoC}_{\text{bat}}^{t-1} + \frac{P_{\text{bat}}^t T}{\eta_{\text{bat}} \text{Cap}_{\text{bat}}} \quad (10b)$$

$$\text{SoC}_{\text{bat}}^{t=0} = \text{SoC}_{\text{bat}}^{t=24} \quad (11)$$

$$\text{SoC}_{\text{bat,min}} < \text{SoC}_{\text{bat}}^t < \text{SoC}_{\text{bat,max}} \quad (12)$$

$$-P_{\text{bat,rated}} < P_{\text{bat}}^t < P_{\text{bat,rated}} \quad (13)$$

B. Control Methods for Voltage Fluctuation Mitigation

To realize the controllability advantage of the SST and the HT, an appropriate voltage control method is essential. On the LV side, the feeder-end voltage V_{fe} fluctuation can be regulated by adjusting the feeder-head voltage V_{fh} , which is $V_{\text{HT_fh}}$ for the HT in (1) and $V_{\text{SST_fh}}$ for the SST in (2). The decentralized control method in Fig. 3 does not require a grid model, but V_{fe} needs to be measured and communicated. Note that if V_{fe} is not measured, currents from each feeder node and an accurate grid model would be required to estimate V_{fe} . However, an accurate model is normally not available from the utility [68]. Thus, further reducing the communication burden is nontrivial. In Fig. 3 (a), an integral controller with deadband and saturation limit is proposed. In each control cycle, only when the feeder-end voltage V_{fe} is out of the deadband $[V_{\text{LV_db,min}}, V_{\text{LV_db,max}}]$, the converter voltage V_{conv} ($V_{\text{SST_conv}}$ for the SST and $V_{\text{HT_conv}}$ for the HT) is adjusted in (14) by one step V_{step} , i.e., 0.01 pu in the simulations. The converter voltage V_{conv} should be adjusted in (15) so that the feeder-head voltage V_{fh} in (16)-(17) is within the limits $[V_{\text{LV,min}}, V_{\text{LV,max}}]$ as dictated by the grid code. Moreover, the converter output voltage should not exceed the

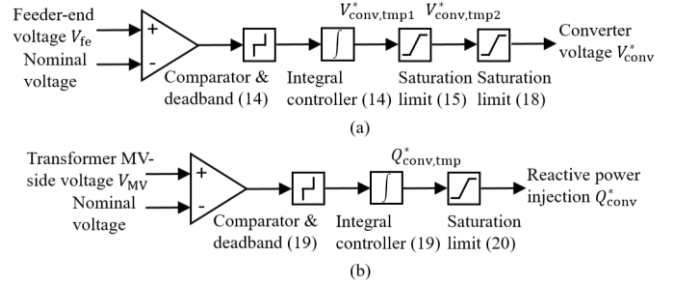


Fig. 3. Control block diagrams for the hybrid transformer (HT) and the solid-state transformer (SST) to regulate (a) the LV-feeder-side voltage and (b) the MV-grid-side voltage.

voltage rating as given by (18). In the HT, $V_{\text{HT_conv}}$ cannot exceed the partially-rated converter rating $V_{\text{HT_conv,rated}}$.

$$V_{\text{conv,tmp1}}^{*,t} = \begin{cases} V_{\text{conv}}^{*,t-1} + V_{\text{step}}, & \text{if } V_{\text{fe}}^{t-1} < V_{\text{LV_db,min}} \\ V_{\text{conv}}^{*,t-1} - V_{\text{step}}, & \text{if } V_{\text{fe}}^{t-1} > V_{\text{LV_db,max}} \\ V_{\text{conv}}^{*,t-1}, & \text{otherwise} \end{cases} \quad (14)$$

$$V_{\text{conv,tmp2}}^{*,t} = \begin{cases} V_{\text{conv,tmp1}}^{*,t} + V_{\text{LV_db,min}} - V_{\text{fh}}^{*,t}, & \text{if } V_{\text{fh}}^{*,t} < V_{\text{LV_db,min}} \\ V_{\text{conv,tmp1}}^{*,t} + V_{\text{LV_db,max}} - V_{\text{fh}}^{*,t}, & \text{if } V_{\text{fh}}^{*,t} > V_{\text{LV_db,max}} \\ V_{\text{conv,tmp1}}^{*,t}, & \text{otherwise} \end{cases} \quad (15)$$

$$V_{\text{HT_fh}}^{*,t} = V_{\text{HT_conv,tmp1}}^{*,t} + V_{\text{HT_sec}}^{t-1} \quad (16)$$

$$V_{\text{SST_fh}}^{*,t} = V_{\text{SST_conv,tmp1}}^{*,t} \quad (17)$$

$$V_{\text{conv}}^{*,t} = \begin{cases} V_{\text{conv,rated}}, & \text{if } V_{\text{conv,tmp2}}^{*,t} > V_{\text{conv,rated}} \\ V_{\text{conv,tmp2}}^{*,t}, & \text{otherwise} \end{cases} \quad (18)$$

On the MV side, reactive power injection into the MV grid can be controlled to regulate the voltage of the targeted bus and positively affect nearby buses, which can mitigate voltage fluctuations when PV is installed at these buses. The proposed MV-side volt/var control is illustrated in Fig. 3 (b). The targeted bus voltage is chosen to be the MV-side voltage of the MV/LV transformer to enable decentralized control with only local information and minimal communication burden. Moreover, the grid model is not required, which is desirable because the network impedance model is generally not available [68]. In (19), when the targeted bus voltage V_{MV} is outside of the deadband $[V_{\text{MV_db,min}}, V_{\text{MV_db,max}}]$, the reactive power injection Q_{conv} ($Q_{\text{SST_conv}}$ for the SST and $Q_{\text{HT_conv}}$ for the HT) is adjusted by one step Q_{step} , i.e., 10 kvar for the SST and 1 kvar for the HT in the simulations. When the targeted bus voltage V_{MV} is within the deadband, the reactive power injection remains unchanged in (19). Moreover, the reactive power injection cannot exceed the total power rating of the converter $S_{\text{conv,rated}}$ as given in (20)-(21).

$$Q_{\text{conv,tmp}}^{*,t} = \begin{cases} Q_{\text{conv}}^{*,t-1} - Q_{\text{step}}, & \text{if } V_{\text{MV}}^{t-1} < V_{\text{MV_db,min}} \\ Q_{\text{conv}}^{*,t-1} + Q_{\text{step}}, & \text{if } V_{\text{MV}}^{t-1} > V_{\text{MV_db,max}} \\ Q_{\text{conv}}^{*,t-1}, & \text{otherwise} \end{cases} \quad (19)$$

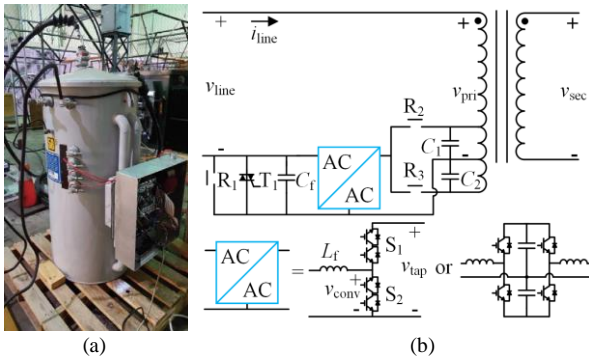


Fig. 4. (a) Experimental prototype and (b) circuit diagram of a 7.2 kV 50 kVA hybrid transformer with $\pm 5\%$ secondary-voltage controllability.

TABLE II
Parameters of the 7.2 kV hybrid transformer (HT) prototype

Parameter	Symbol	Value
Switching frequency	f_{sw}	5 kHz
Bidirectional switches from anti-series Si IGBTs	S_1, S_2	1.2 kV, 25 A
Relay	R_1	400 V, 120 A
Relay	R_2, R_3	300 V, 20 A
Bidirectional fail-normal switches from paralleled thyristors	T_1	1.4 kV, 180 A
Filter inductor	L_f	20 mH
Filter capacitor	C_f	2.2 μ F
Filter capacitor	C_1, C_2	10 μ F

$$Q_{conv}^{*,t} = \begin{cases} -Q_{conv,tmp}^{*,t}, & \text{if } Q_{conv,tmp}^{*,t} < -Q_{conv,sat}^{*,t} \\ Q_{conv,tmp}^{*,t}, & \text{if } Q_{conv,tmp}^{*,t} > Q_{conv,sat}^{*,t} \\ Q_{conv,tmp}^{*,t}, & \text{otherwise} \end{cases} \quad (20)$$

$$Q_{conv,sat}^{*,t} = \sqrt{S_{conv,rated}^2 - P_{conv}^{*,t}^2} \quad (21)$$

Besides the advantages of minimal communication burden and no required knowledge of the grid model, the control methods feature deadband to reduce the possibility of oscillation and interaction. Due to the deadband, the possible equilibrium points are a set instead of a single operating point.

V. MEDIUM-VOLTAGE SOLID-STATE TRANSFORMER AND HYBRID TRANSFORMER EXPERIMENTAL PROTOTYPES

Before the assessments of the HT and SST in distribution grids, their technical feasibility is verified by MV experimental results from a HT prototype and a SST prototype. The MV waveforms from a MV/LV distribution HT prototype and voltage controllability are scarce in the literature and reported for first time, to the authors' best knowledge.

A. Hybrid Transformer (HT)

A 7.2 kV/240 V HT prototype in Fig. 4 has been built and tested. In this prototype, the partially-rated converter is a direct AC-AC converter on the MV side of the transformer to avoid bulky DC-link capacitors for reduced cost, high reliability, and long lifetime. A conventional back-to-back voltage-source converter is an alternative solution [55]. In Fig. 4, the basic operation principle is to inject a voltage V_{conv} by switching S1

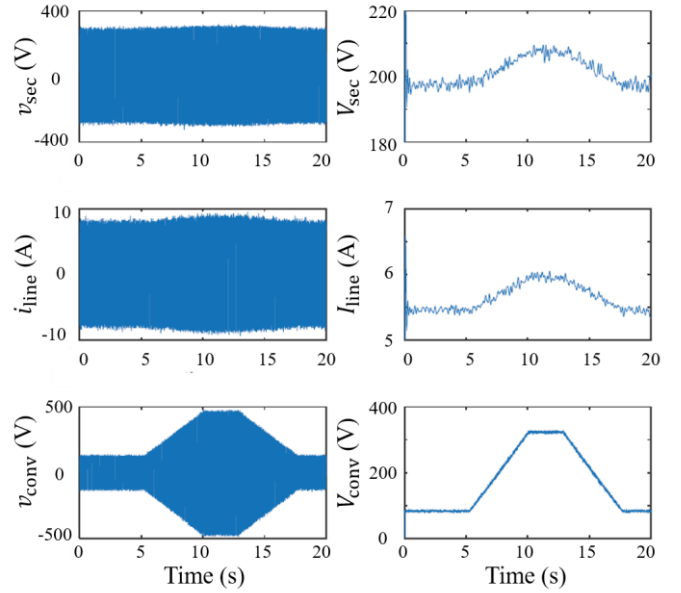


Fig. 5. Experimental waveforms of the hybrid transformer prototype at 6.2 kV for 5% secondary-voltage boost operation.

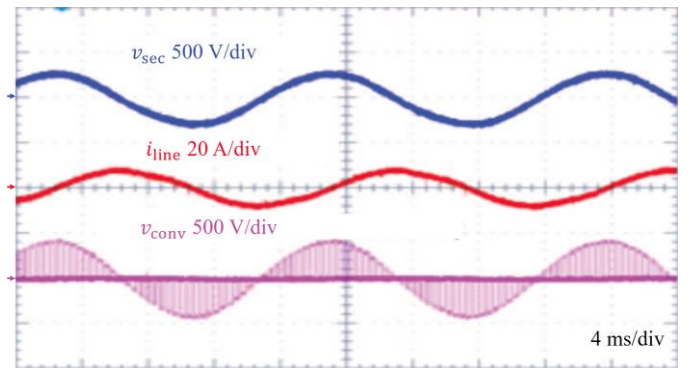


Fig. 6. Zoomed experimental waveforms of the hybrid transformer prototype at 6.2 kV with 10% duty cycle for boost operation.

and S2 alternatively in the direct AC-AC chopper with any duty cycle, i.e., S1 conducting duration, between 0% and 100% [69]. The injected voltage V_{conv} can adjust the voltage V_{pri} across the primary winding of the transformer to change the secondary-winding voltage V_{sec} for a LV feeder. With the dual virtual quadrature source control [70], reactive power support can also be achieved. During normal operation, the fail-normal switch R1 and T1 are open. When the converter fails or short-circuit fault current sourcing is needed to inform legacy protection relays, the fail-normal switch R1 and T1 are closed to bypass the converter. The converter is designed for $\pm 5\%$ voltage regulation capability with the parameters listed in Table II.

The waveforms at 6.2 kV MVAC in Fig. 5 illustrate the 5% boost operation, where the relay R2 is closed and R3 is open. The left half of Fig. 5 shows real-time measurements, and the right half of Fig. 5 illustrates rms values. In Fig. 5, the transformer secondary-side voltage is smoothly ramped up from roughly 200 V to 210 V and then ramped back down to

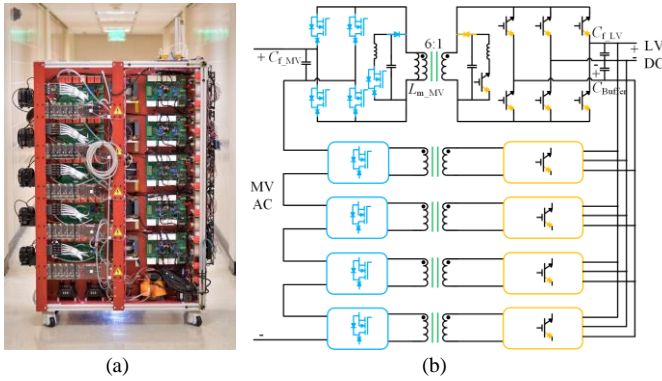


Fig. 7. Schematic and experimental prototype of a 7.2 kV 50 kVA AC/DC modular solid-state transformer.

TABLE III

Parameters of the 7.2 kV solid-state transformer (SST) prototype

Parameter	Symbol	Value
Switching frequency	f_{sw}	16 kHz
Magnetizing inductance	L_{m_MV}	6.5 mH
Filter capacitor	C_{f_MV}	2.0 μ F
Filter capacitor	C_{f_LV}	80.0 μ F
Buffer capacitor	C_{Buffer}	5.3 mF
MV SiC MOSFETs and SiC diodes	—	3.3 kV, 45 A
LV Si IGBTs and SiC diodes	—	650 V, 150 A

200 V, as the injected converter voltage is ramped up from roughly 100 V to 300 V and then back down to 100 V. Fig. 6 shows the partially-rated converter's output voltage V_{conv} during the voltage ramp up when the duty cycle is 10%. In summary, the voltage regulation capability and the technical feasibility of a HT are verified in Figs. 5-6 at 6.2 kV.

B. Solid-State Transformer (SST)

A 7.2 kV modular SST prototype is shown in Fig. 7 with parameters listed in Table III. This SST is a current-source converter, where the transformer magnetizing inductance L_{m_MV} is the current DC link. Hence, the SST can operate under AC/AC or AC/DC or DC/DC mode [14]. As the major challenge of the SST lies in the MV and isolated stage, demonstrating MVAC to LVDC conversion is desirable [27], [34], [43]. A standard LV inverter can be used for a regulated LV AC voltage.

In Fig. 8, single-module operation at 1.44 kV is shown, where the MV side and the LV side of the SST are connected to a resistor bank and a rectifier, respectively. The MVAC voltage v_{Cf_MV} is sinusoidal. The LVDC voltage v_{Cf_LV} is smooth and steady. The buffer voltage v_{C_Buffer} has a double-line-frequency ripple as the buffer capacitors absorb the double-line-frequency power ripple under the single-phase loading condition. Larger buffer capacitance or additional filters are needed to fulfill ripple requirements, if interfacing a battery on this port is desired. Note that the double-line-frequency voltage of v_{C_Buffer} is internal and does not affect the external MVAC characteristics. In summary, the performance and the technical feasibility of a SST are verified at MV.

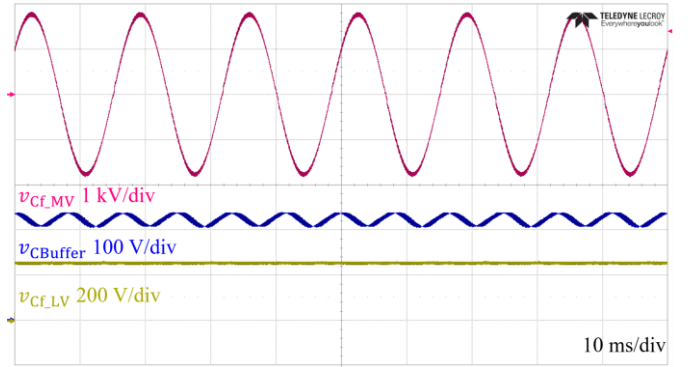


Fig. 8. Single-module waveforms of the solid-state transformer at 1.44 kV.

VI. TECHNICAL IMPACT EVALUATION OF SOLID-STATE TRANSFORMER AND HYBRID TRANSFORMER IN ACTIVE DISTRIBUTION GRIDS

A. Simulation Methods

Comprehensive simulations have been carried out to determine the PV hosting capacity in both the LV feeder and the MV networks, the impacts of the BESS and the controllability, and the yearly operational cost of the LV feeder, when the MV/LV transformer in Fig. 1 is a HT, a SST, or a LFT. The simulations are based on the dispatch and control methods in Section IV. The location under study is Atlanta, and the corresponding yearly load profiles and PV generation profiles are from [71]-[72]. The SST and the integrated BESS power ratings are sized based on the peak power of the LV feeder over the entire year, which is 103.8 kW on phase B on August 19. Thus, the three-phase rating of the SST is selected to be 360 kW with ~15% margin. The BESS is sized to be 360 kW 720 kWh with a duration of 2 hours, according to the average US utility BESS duration of 1.7 hours [73]. The HT has a fractional converter rating of 12 kW per phase and the integrated BESS is 12 kW 24 kWh. While this section reports the results of one set of parameters, the fractional converter rating of the HT and the BESS duration of the HT and the SST will be swept to comprehensively study the system-level economic impacts in Section VII. The LV and MV PV hosting capacities for each of the three transformer types are determined by incrementally increasing the PV penetrations until any of the following constraints are violated: LV-node voltages outside of the ANSI C84.1 limits of [0.95 pu, 1.05 pu] for $[V_{LV,min}, V_{LV,max}]$, MV-node voltages outside of the ANSI C84.1 limits of [0.975 pu, 1.05 pu] for $[V_{MV,min}, V_{MV,max}]$, reverse power flow into the upstream MV grid due to the absence of the BESS to buffer PV power (for the LFT case) and the finite power rating of the BESS (for the HT and SST cases). Note that because the MV-grid voltage fluctuation can fully or partially propagate into the LV-feeder when the LFT or the HT is used, the MV PV hosting capacity is coupled to the LV PV hosting capacity. To address this issue, the following strategy is used. The MV PV power is first set to zero and the LV PV power is gradually increased until the maximum LV hosting capacity is reached. Then, the LV PV power is set at the hosting

TABLE IV

LV-Feeder PV Hosting Capacity with Line-Frequency Transformer (LFT), 10% Hybrid Transformer (HT), and Solid-State Transformer (SST)

Node	Phase	SST (kW)	HT (kW)	LFT (kW)
2	A	42.25	13.00	7.15
4	B	19.50	6.00	3.30
5	B	19.50	6.00	3.30
Total LV-Feeder PV		81.25	25.00	13.75

TABLE V

MV-Grid PV Hosting Capacity with Line-Frequency Transformer (LFT), 10% Hybrid Transformer (HT), and Solid-State Transformer (SST)

Node	SST (kW)	HT (kW)	LFT (kW)
832	70.00	53.00	51.50
858	105.00	79.50	77.25
834	140.00	106.00	103.00
Total MV-Grid PV	315.00	238.50	231.75

capacity, and the MV PV power is gradually increased to determine the MV PV hosting capacity under the maximum LV PV. The deadband of the voltage control is selected close to the voltage violation limits to reduce operation frequency and the possibility of converter interaction, and within the voltage violation limit to allow voltage fluctuation mitigation. The deadband is selected to be $[0.98 \text{ pu}, 1.045 \text{ pu}]$ for $[V_{MV_db_min}, V_{MV_db_max}]$ and $[0.96 \text{ pu}, 1.045 \text{ pu}]$ for $[V_{LV_db_min}, V_{LV_db_max}]$. Finally, the obtained LV and MV PV hosting capacities are shown in Tables IV and V, respectively.

In the following subsections, simulation results are shown for the worst-case day of the year in terms of grid-edge voltage fluctuation and reverse power flow with the maximum possible PV installed in Tables IV and V. Using the aforementioned load and PV profiles [71]-[72], the worst-case day is determined to be May 27, as this day featured the largest negative net load (load minus PV generation) over the year due to high PV generation and low load consumption. May 27 is close to summer, which agrees with the literature [74]. The PV and load profiles for the worst-case day are given in Fig. 9.

B. Solid-State Transformer (SST)

The day-ahead optimal dispatch plan of the integrated BESS in the SST is shown in Fig. 10. The total power from the MV grid is scheduled to be non-negative to prevent the reverse power flow. Note that the optimal dispatch considers the electricity cost which is higher during afternoon and lower during morning and night, and the demand charge, which penalizes large peak power spikes. Hence, in Fig. 10, the total power from the MV grid is smooth without sharp spikes and the battery is scheduled to make the total power drawn from the grid very small in the afternoon to reduce the electricity cost. Fig. 11 illustrates the real-time operation of the BESS compared

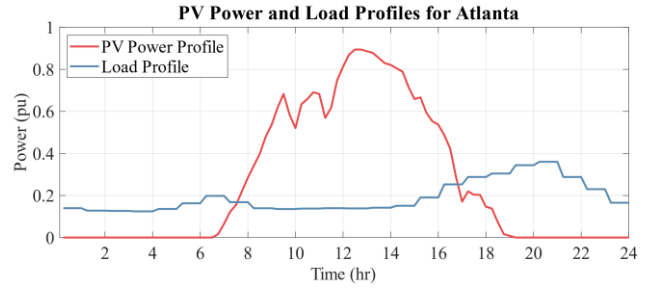


Fig. 9. PV power and load power profiles in Atlanta [72]-[73]. The profiles correspond to the selected worst-case day (May 27) in terms of LV-feeder overvoltage conditions. This day is used for the further simulations.

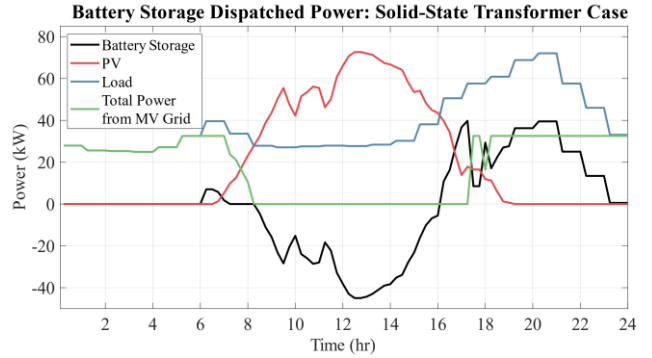


Fig. 10. Day-ahead dispatch plan of the BESS inside the solid-state transformer (SST). PV power, active power of the load, active power drawn from the MV grid, and the optimal dispatch plan of the BESS are shown.

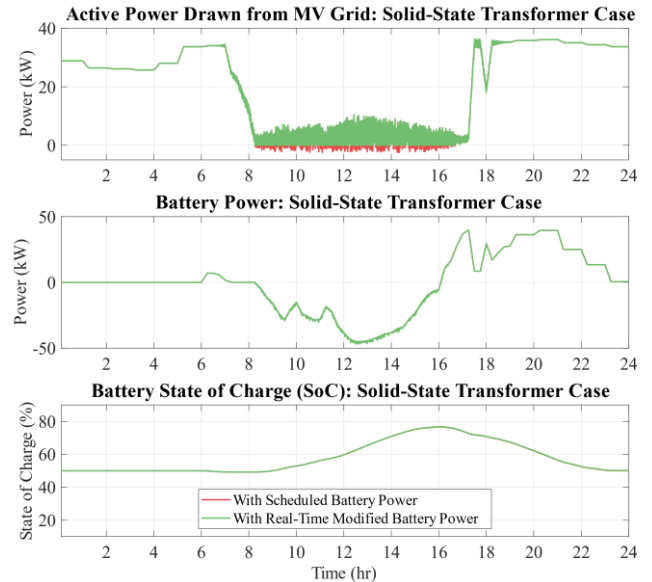


Fig. 11. Real-time operational results of the SST and the integrated BESS. A 10% PV forecasting error between the day-ahead dispatch plan and the real-time operation is added on the PV power output. Reverse power flow into the MV grid is prevented in real-time by adjusting the BESS power to compensate for the PV forecasting error.

to the optimal dispatch. A 10% stochastic noise is added to the PV power profile in the day-ahead dispatch planning to test the performance of the system under some PV power forecasting error. The real-time BESS power is adjusted to vary slightly

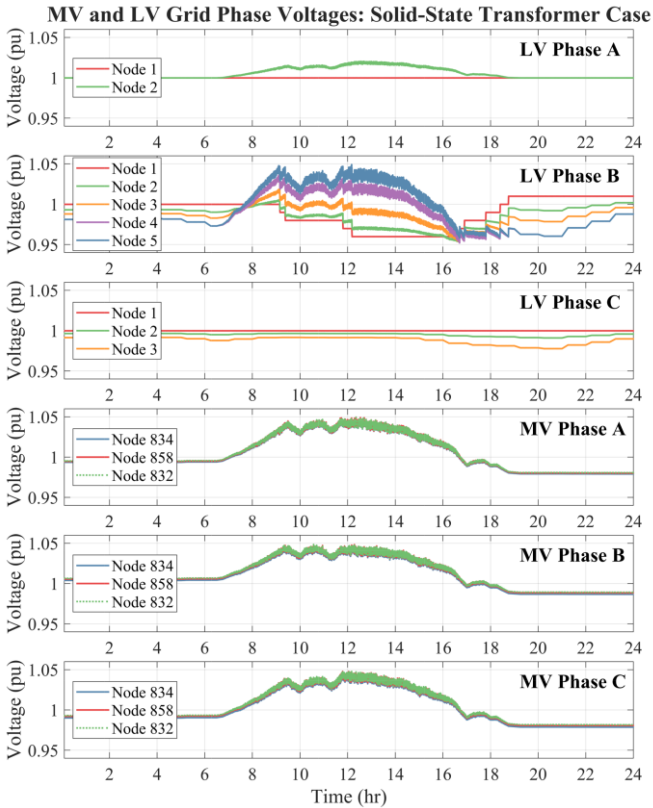


Fig. 12. Voltage profiles of the LV feeder and the MV grid in the solid-state transformer (SST) case. The SST provides 100% LV-side and MV-side voltage control. There is an integrated BESS inside the SST of the same power rating as the SST.

from the dispatch plan to compensate for the variability and to prevent reverse power flow in Fig. 11.

The LV and MV voltage profiles with the SST as the MV/LV interface transformer are shown in Fig. 12. For the LV feeder, when the PV generation peaks during mid-day, the SST reduces the feeder-head node 1 voltage to prevent grid-edge overvoltage. Around 17:00, with falling PV production and increasing load consumption, the SST quickly increases the feeder-head node 1 voltage to prevent grid-edge undervoltage. The LV feeder is close to the maximum PV hosting capacity as the node 1 and 5 voltages are close to the ANSI limits. For the MV grid, volt/var support is implemented. The reactive power injection is adjusted to ensure the ANSI limits are satisfied. At mid-day in Fig. 12, the MV-grid voltage is very close to the ANSI limits, while the SST's reactive power support is at its maximum and limited by the physical kVA rating, which is why the MV PV cannot be further increased. Note that the SST LV feeder-head node 1 voltage for phase A is flat during mid-day when the PV on the MV grid peaks, which means that the LV-feeder voltage is decoupled from the MV-grid voltage to certain extent in the SST. In other words, the MV voltage fluctuation will not affect the LV PV penetration when the SST serves as the MV/LV transformer, while the same is not true for the HT and the LFT.

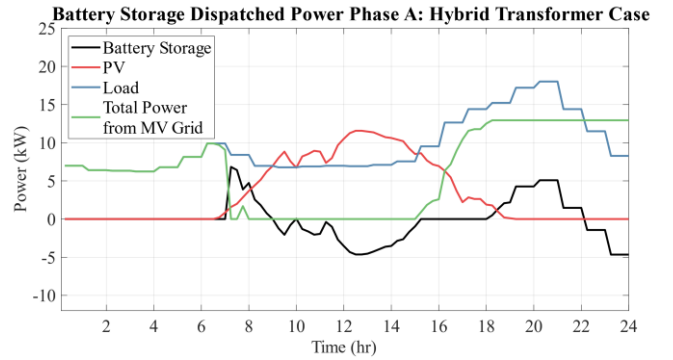


Fig. 13. Day-ahead dispatch plan of the BESS inside the hybrid transformer (HT) on phase A. PV power, active power of the load, active power drawn from the MV grid, and the optimal dispatch plan of the BESS are shown.

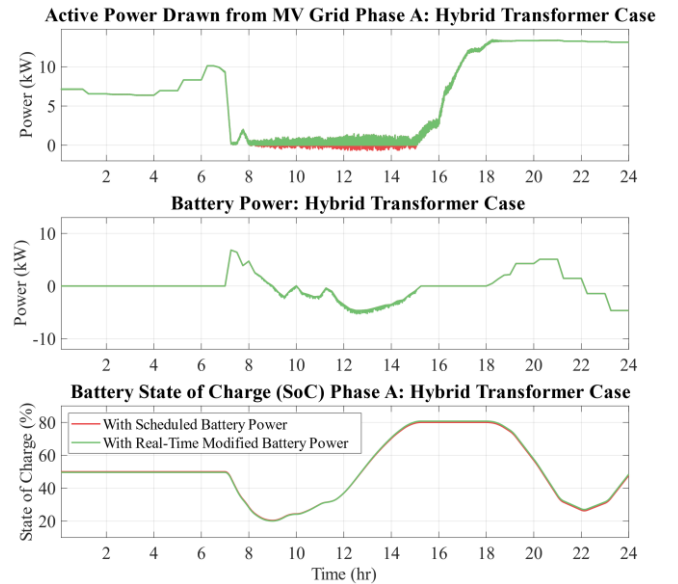


Fig. 14. Real-time operational results of the HT and the integrated BESS on phase A with a 10% PV forecasting error between the day-ahead dispatch plan and the real-time operation.

C. Hybrid Transformer (HT)

The optimal dispatch and the real-time operation of the BESS in phase A of the HT are shown in Figs. 13-14. In Fig. 13, the optimal dispatch schedules the BESS to smooth out the active power drawn from the MV grid to avoid power spikes and large demand charges. Also, the BESS is dispatched so that the electricity consumption from the MV grid is small during the afternoon when the electricity price is high to reduce the cost. In Fig. 14, the forecasting error of the PV is compensated by the BESS, and upstream reverse power flow into the MV grid is prevented, similar to the case of the SST.

The LV and MV voltage profiles with the HT as the MV/LV interface transformer are illustrated in Fig. 15. Note that though the power converter inside the HT can inject an additional voltage on top of the MV-side voltage to regulate the LV-side output voltage, the MV-grid voltage and the LV-feeder-head node 1 voltage are not fully decoupled. This phenomenon can be observed in the LV-grid phase A voltage of Fig. 15 which follows the same pattern as the MV-grid phase A voltage, while

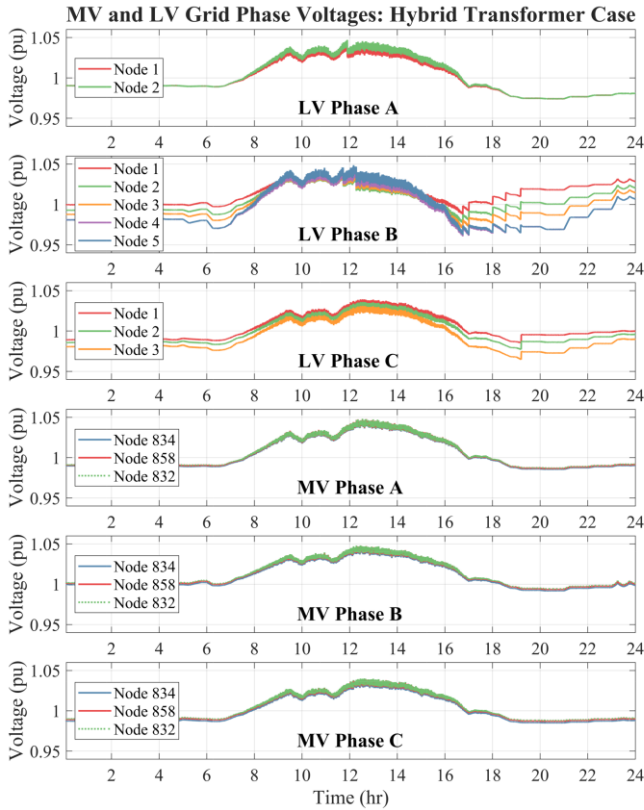


Fig. 15. Voltage profiles of the LV feeder and the MV grid in the hybrid transformer (HT) case. The HT provides 10% LV-side and MV-side voltage control up to its fractional kVA rating (10% of the SST). The integrated BESS inside the HT also has 10% of the power rating of the BESS in the SST.

the same is not true for the SST in Fig. 12. This is one reason why the HT has less PV hosting capacity than the SST, as shown in Tables IV and V. The other reason is that the excess energy produced by the PV needs to be stored in the BESS to prevent the reverse power flow due to the incompatibility with legacy protection system and the issue of power back-feeding policy [1], [65]. With the 100% rated, 2-hour BESS in the SST in Fig. 11, the BESS is charged to store the extra PV energy from ~ 0.5 SoC to ~ 0.8 SoC. However, the power and energy rating of the BESS in the HT is physically limited with the partially-rated converter architecture and is only 10% of that in the SST, which compromises the PV hosting capacity.

D. Line-Frequency Transformer (LFT)

In the case of the LFT, the LV and the MV voltage profiles are shown in Fig. 16. Due to the lack of the voltage control from the converters and the buffering from the integrated BESS, the voltage profiles reach the ANSI limits, and the reverse power flow occurs at significantly lower PV penetrations than the SST or the HT case, as shown in Tables IV and V. Furthermore, even with no PV power at 20:00, the LV grid phase B voltage has already violated the ANSI limits due to the peak load consumption at night in Fig. 9. Traditionally, when an LV feeder has a low PV penetration, LTCs are used to address this under-voltage violation. However, suffering from the short lifetime under high PV penetration, the LTCs are disabled in

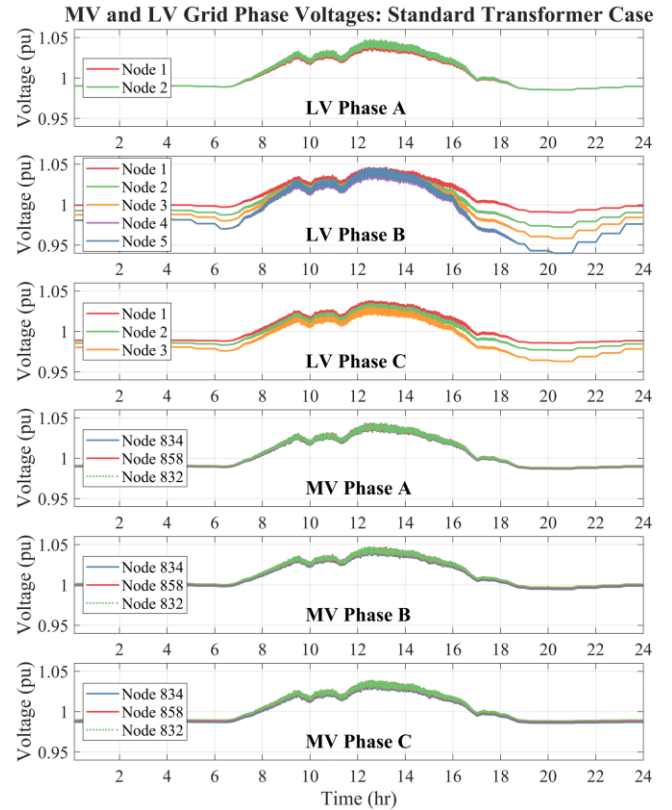


Fig. 16. Voltage profiles of the LV feeder and the MV grid in the standard line-frequency transformer (LFT) case. There is no LV-side voltage control or MV-side reactive power control in this case.

the simulations as previously mentioned.

E. Summary of Technical Benefits and Operation Costs

For clarity, the key differences between the voltage profiles in Figs. 12, 15, 16 are emphasized here. On the LV side, the SST enables full decoupling between the MV and the LV voltages, which is why the LV node 1 voltages are flat in Fig. 12. The HT and the LFT can only achieve partial and no decoupling, respectively. The LV node 1 voltages in Figs. 15-16 thus show fluctuations propagated from the MV grid. Furthermore, the controllability from the SST and the HT enables increasing the LV node 1 phase B voltages rapidly around 18:00 to prevent the LV node 5 undervoltage in Figs. 12 and 15. The LFT suffers from this feeder-end undervoltage issue in Fig. 16. On the MV side, the shapes of the voltage profiles are similar in Figs. 12, 15, 16, because the same PV profile is used. However, the MV PV hosting capacity is significantly different as shown in Table V.

Concerning technical benefits, compared to the LFT, the SST and the HT with integrated BESS can achieve peak shaving, reverse power flow mitigation, energy arbitrage, and voltage fluctuation mitigation. The peak MV-grid power in the simulations for the SST, the HT, and the LFT are 36.38 kW, 58.66 kW, and 75.66 kW, respectively. Then, the benefits of peak load shaving of 51.92% by the SST and 22.47% by the HT can help asset lifetime extension [7]. Mitigation of reverse power flow can alleviate the incompatibility with legacy

protection methods and electricity market policy [1], [65]. Lastly, energy arbitrage can be used to reduce the operational cost.

In addition, the voltage-fluctuation mitigation capability of the SST allows a significantly higher penetration of PV on both the MV network by 35.92% and the LV network by 490.91% compared to the LFT as shown in Tables IV-V, while still meeting the ANSI voltage limits on both sides. The HT also achieves improved LV PV hosting capacity compared to the LFT by 81.82%. The reader may wonder why the hosting capacity gain of the MV PV is much less than the LV PV. The distribution networks are much more resistive compared to the transmission networks, which means that the MV voltage is less sensitive to reactive power, and much more var injection is needed to adjust the voltage. On the other hand, the LV feeder voltage is controlled effectively by adjusting the converter output and changing the feeder-head voltage, not by var. Note that the amount of the hosted PV in this article is limited by the voltage and the reverse-power constraints, not by the line thermal capacity.

Furthermore, for the simulated system, the SST with yearly operation cost \$30,006 and the HT with yearly operation cost \$36,043 offer cost reductions of 21.05% and 5.16%, respectively, compared to the LFT with yearly operation cost \$38,004. The operational cost is calculated from the LV feeder perspective, and the volt/var support is provided to the external MV grid. The pricing in distribution grids of ancillary services such as reactive power support is still an open question [75]. Therefore, the benefits of increased MV PV hosting capacity are not included in the operational cost calculation. Note that the operational cost savings are achieved in conjunction with the aforementioned technical benefits, thanks to the controllability and the flexibility of the power converters and the integrated storage in the SST and HT.

VII. ECONOMIC ASSESSMENT AND COMPARISON OF SOLID-STATE TRANSFORMER AND HYBRID TRANSFORMER

To analyze the economics of the SST and the HT relative to the LFT, net present value (NPV) and internal rate of return (IRR) are calculated. The NPV considers the cumulative impact of income cash flows (CF_t) each year over the project duration (T) with annual discount rate (r) versus initial capital cost (C_0). A negative NPV means that the project is not financially profitable.

$$NPV = -C_0 + \sum_{t=1}^T CF_t(1+r)^{-t} \quad (22)$$

The IRR computes the projected return rate of the project, corresponding to the rate that makes NPV zero. A higher IRR, e.g., more than 5%-10%, leads to an equivalently higher annual return rate for the investment in the project.

$$-C_0 + \sum_{t=1}^T CF_t(1+IRR)^{-t} = 0 \quad (23)$$

The capital costs of different equipment are listed in Table VI. The SST cost of 86.2 \$/kVA and the HT cost of 31.7 \$/kVA are estimated from the MV prototypes in Section V. Because the lifetime of the BESS is 10 years and one replacement over the 20-year project duration (T) is needed, the BESS cost is doubled to be 380 \$/kWh [77]. The PV system cost is 1.83 \$/W

TABLE VI
Capital Cost of Different Equipment

Equipment	Cost
Solid-state transformer	86.2 \$/kVA
Hybrid transformer	31.7 \$/kVA
Line-frequency transformer	25 \$/kVA
PV generation system	1830 \$/kW
Battery energy storage system	190 \$/kWh

TABLE VII
LV-Feeder PV Hosting Capacity of Solid-State Transformer (SST) and Hybrid Transformer (HT) under Different Converter and Storage Ratings

Storage (hr)	SST (kW)	HT (kW)		
		10%	15%	20%
0.5	62.50	18.75	20.00	21.25
1.0	81.25	21.25	22.50	23.75
2.0	81.25	25.00	27.50	30.00
4.0	81.25	30.00	36.25	41.25

[78]. The sum of all equipment costs determines the initial capital cost (C_0). The income cash flow (CF_t) each year is the yearly benefits of replacing the LFT with the SST or the HT, i.e., yearly operational cost reduction of the SST or the HT case compared to the LFT. For example, \$30,006, \$36,043, and \$38,004 are the yearly operational cost of the SST, HT, and LFT cases under the parameters of the simulation section, respectively. Note that as the PV hosting capacity has been verified through the simulations with the proposed control, the voltage constraints, the reverse-power-flow constraints, etc., are satisfied under this set of parameters. The yearly operational cost numbers are calculated by adding up the daily operational cost optimization results in (7) throughout a year. Then, the yearly operational cost reduction of the SST and the HT in this case are calculated as \$7998 and \$1961, respectively, as compared to the LFT. The annual discount rate (r) is 5% [76]. The PV hosting capacity is summarized in Table VII, where the partial converter rating inside the HT is swept from 10% to 20%. The BESS power rating inside the HT is the same as the partial converter rating. In these cases, the PV hosting constraints are voltage fluctuations outside the limits and energy storage requirements to prevent reverse power flow. For the HT cases, the energy storage constraint dominates. When the BESS power and energy (duration) ratings in the HT cases increase, the hosting capacity increases. The PV hosting capacity of the SST increases with the BESS energy rating until 81.25 kW. Beyond 81.25 kW, the voltage constraint dominates, which is why further increasing the SST storage duration from 1 hour to 4 hours cannot increase the PV hosting capacity, as in Table VII.

Based on the data and parameters above, the IRR of the SST and the HT is depicted in Fig. 17 across a range of PV

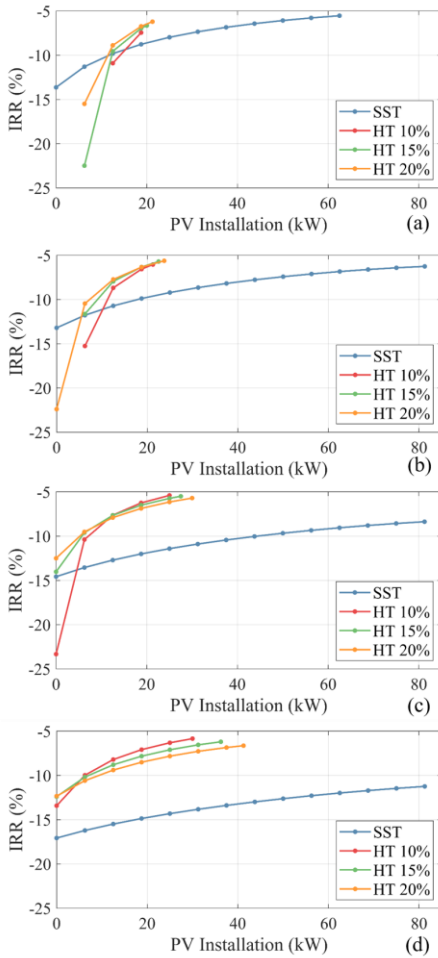


Fig. 17. IRR of the SST and the HT with different controllability under (a) 0.5 hour, (b) 1 hour, (c) 2 hours, and (d) 4 hours storage duration across a range of PV installation up to their PV hosting capacities. At some points with very small BESS and PV, and poor profitability, IRRs can become complex numbers and not plotted, e.g., HT 10% 0 kW PV in Fig. 17 (a), while the LFT can host a small amount of PV as in Table IV.

installation up to the corresponding PV hosting capacity, where the fractional converter rating inside the HT is swept from 10% to 20% and the BESS duration is swept from 0.5 hour to 4 hours. First, it can be observed that the HT and the SST are not yet economically viable in this use case with the IRR below zero. Second, with the increase of PV installation, the IRR increases in Fig. 17 (a)-(d). However, the slope of the IRR trace becomes more flat when the installed PV increases. In fact, the effort of accommodating the same incremental amount of PV, i.e., voltage regulation and storage to prevent reverse power flow, increases when the installed PV approaches the hosting capacity limit and the marginal benefit of PV decreases, resulting in a more flat slope. Third, with PV penetration around 18 kW, the 10% HT is economically better with higher IRR in Fig. 17 (b)-(d) for 1, 2, 4 hours storage, compared to the larger power converter solutions like 20% HT or the SST. Because the average US utility BESS duration is 1.7 hours [73], the 10% HT can then be regarded as generally better than the 15% or 20% HTs for the use case discussed. Fourth, to realize the highest

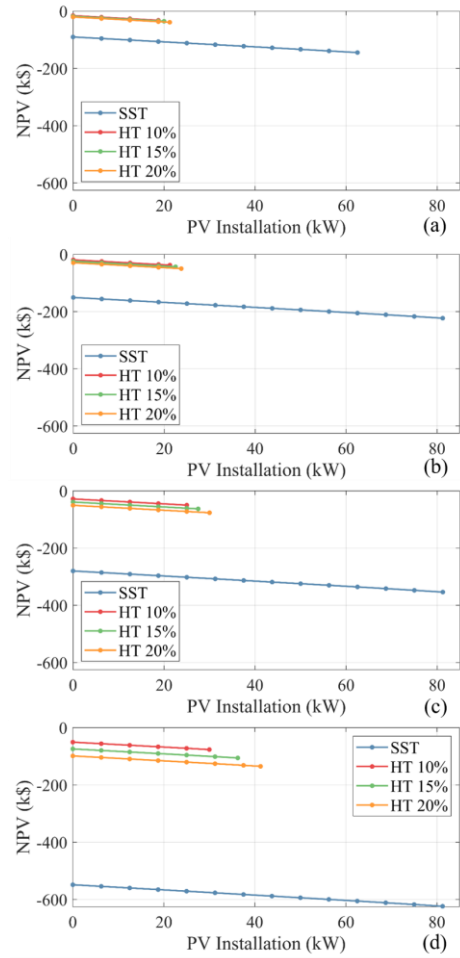


Fig. 18. NPV of the SST and the HT with different controllability under (a) 0.5 hour, (b) 1 hour, (c) 2 hours, and (d) 4 hours storage duration across a range of PV installation sizes up to the corresponding PV hosting capacities.

possible PV penetration around 80 kW, the SST is needed due to the aforementioned reverse-power-flow-related protection and market issues. However, the economic viability of the SST is not as good with an IRR lower than -6% in Fig. 17 (b) and -11% in Fig. 17 (d).

The NPV with different HTs and the SST across different installed PV power and storage durations is portrayed in Fig. 18. Since the IRR is always negative under the same scenario in Fig. 17, projects with larger capital investments like longer-duration storage or more PV installations will have more negative NPV. Under the same PV installation, the NPV of the SST is the most negative, because of the largest integrated BESS and higher capital cost compared to the HT. In fact, as can be observed in Table VI, the unit costs of the BESS and the PV are much higher than the LFT, the HT, or the SST, dominating the initial capital cost.

The sensitivities of the IRR to $\pm 80\%$ PV cost variation and $\pm 80\%$ BESS cost variation are shown in Fig. 19 and Fig. 20, respectively. First, all the solutions including the SST and the HT have better IRR with reduced PV or BESS cost. Second, in Fig. 19, the IRR of the SST changes less than 3% with the PV

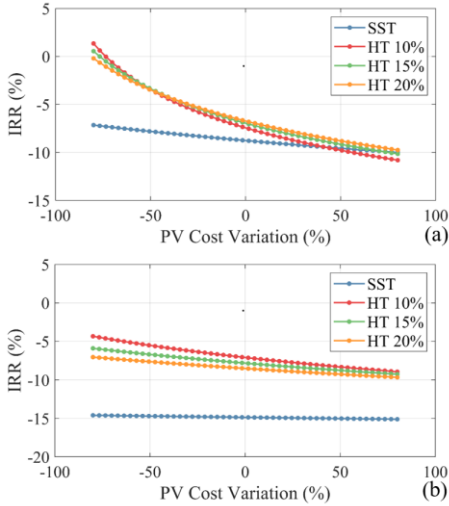


Fig. 19. Sensitivity of the IRR to $\pm 80\%$ PV cost variation. The IRR of the SST and the HT with different controllability and 18.75 kW PV under (a) 0.5 hour and (b) 4 hours storage duration.

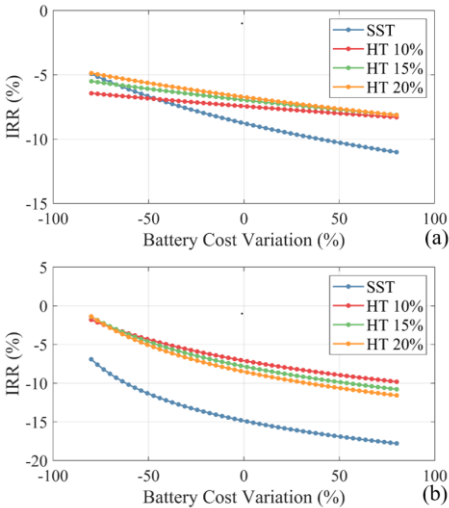


Fig. 20. Sensitivity of the IRR to $\pm 80\%$ battery cost variation. The IRR of the SST and the HT with different controllability and 18.75 kW PV under (a) 0.5 hour and (b) 4 hours storage duration.

cost variation compared to up to 9% with the BESS cost variation. This is because the BESS in the SST is large and accounts for a larger portion of the total capital cost. The opposite holds for the HT, whose IRR is more sensitive to PV cost reduction. Third, though in some cases in Fig. 19 (a), the IRR can turn positive, the IRR still does not reach 5%-10%, which means that the HT and the SST are not economically viable for the studied use case. Fourth, the HT has the highest IRR for most cases in Figs. 19-20. Therefore, the HT generally has better economic viability than the SST with the future PV and BESS cost reduction.

To further investigate the required capital cost reduction or revenue increase to make the SST or the HT solution profitable, the sensitivity of the IRR to the two factors is plotted in Fig. 21.

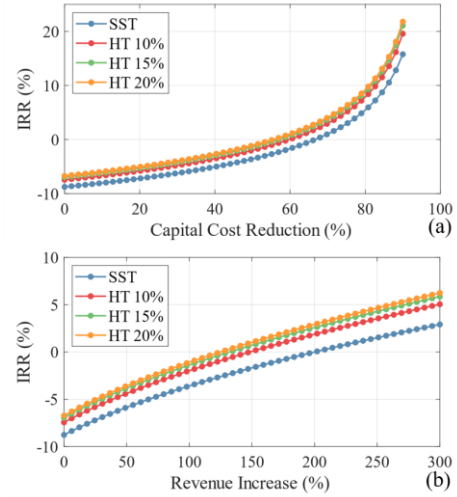


Fig. 21. Sensitivity of the IRR to (a) total capital cost reduction and (b) revenue increase. The IRR of the SST and the HT with different controllability and 18.75 kW PV under 0.5 hour storage duration.

In Fig. 21 (a), under an aggressive 60% total capital cost reduction, the IRR barely turns positive. The IRR is about 10% under 80% total capital cost reduction which is less likely in the next 5-10 years. In Fig. 21 (b), under 150% revenue increase, i.e., yearly benefit increase, the IRR tips above zero.

To summarize, with the studied use case and grid services, the SST and the HT are not yet economically feasible from a system perspective. The HT, especially with a 10% partial converter rating, has better economic metrics in most cases. To make the use case economically viable, either a significant capital cost reduction over 60% is needed or a revenue increase over 150% from more service to the utility is required. From the capital-cost-reduction aspect, the PV and the BESS cost much higher than the SST and the HT, and thus dominate the total system cost, which is the key economic factor for the penetration of the HT and the SST. Significant cost reductions on both PV and storage are needed. From the revenue-generation aspect, more functionalities of the HT and the SST with the integrated storage need to be provided in the future, e.g., resiliency enhancement, frequency regulation, etc. Note that current storage applications in distribution grids do not yet include these services due to implementation, market, or policy issues [7]. Moreover, services such as harmonic filtering and reactive power compensation are not yet priced in the current market [75]. Therefore, the above services are not taken into account in the economic assessment. Besides the equipment-level technical challenges, significant developments are also needed to address the implementation, market, and policy issues to enable a richer set of SST and HT functionalities, along with future cost reduction of PV and BESS systems, for possible economic viability in the utility distribution transformer application.

VIII. CONCLUSION

Solid-state transformer (SST) and hybrid transformer (HT)

are attractive alternatives to the line-frequency transformer (LFT) to mitigate grid-edge voltage fluctuations from increased penetrations of renewable energy sources and electric vehicles and to conveniently integrate energy storage. With most of the work on the SST and the HT focusing on converter level, quantitative technical and economic system-level impacts of the BESS-integrated SST and HT are reported for the first time, to the authors' best knowledge. Experimental waveforms from medium-voltage SST and HT prototypes verify the technical feasibility. Especially, the voltage controllability waveforms of a medium-voltage HT prototype are reported for the first time. Appropriate dispatch and control methods are critical for the SST and the HT to realize the controllability and the storage-integration capability in distribution grids. A voltage control method and a BESS dispatch method are proposed to facilitate the simulations and implementations of the LFT, the SST, and the HT in a modified IEEE 34-bus system. From the simulations, it is found out that the SST and the HT with integrated storage can simultaneously increase PV hosting capacity by 490.91% and 81.82% on the LV feeder, manage voltage fluctuation, achieve peak shaving by 51.92% and 22.47%, prevent reverse power flow, and achieve energy arbitrage for operational cost reduction of 21.05% and 5.16% as compared to the LFT case.

A comprehensive economic assessment on the SST and the HT has been performed in terms of net present value and internal rate of return across different ratings of the HT, ratings of the energy storage, and installed PV power. In addition, sensitivity analysis has been performed for variations in PV, storage, total capital cost, and revenue. Through the assessment, it is found out that the HT and the SST are currently not economically feasible. The 10% HT has better economic metrics in most cases, compared to the 20% HT or the SST. To enable the economic viability of the HT and the SST, further capital cost reduction over 60% and revenue generation increase more than 150% are needed. The decreasing costs of PV and storage, which dominate the system costs, can contribute to the capital cost reduction. Besides equipment-level technical challenges, significant developments are also needed to address the implementation, market, and policy issues to enable more priced grid service opportunities and economic viability in future utility distribution applications of the SST and the HT.

ACKNOWLEDGMENT

The information, data, or work presented herein was funded in part by the Advanced Research Projects Agency-Energy (ARPA-E), U.S. Department of Energy, under Award Number DE-AR0000899 in the CIRCUITS program monitored by Dr. Isik Kizilyalli. The views and opinions of authors expressed herein do not necessarily state or reflect those of the United States Government or any agency thereof.

REFERENCES

- [1] F. Katiraei and J. R. Aguero, "Solar PV integration challenges," *IEEE Power Energy Mag.*, vol. 9, no. 3, pp. 62–71, May/Jun. 2011.
- [2] D. Divan, R. Moghe, and A. Prasai, "Power electronics at the grid edge: The key to unlocking value from the smart grid," *IEEE Power Electron. Mag.*, vol. 1, no. 4, pp. 16–22, Dec. 2014.
- [3] R. Kabiri, D. G. Holmes, B. P. McGrath, and L. G. Meegahapola, "LV Grid Voltage Regulation Using Transformer Electronic Tap Changing, With PV Inverter Reactive Power Injection," *IEEE J. Emerg. Sel. Topics Power Electron.*, vol. 3, no. 4, pp. 1182–1192, Dec. 2015.
- [4] K. Clement-Nyns, E. Haesen, and J. Driesen, "The impact of charging PHEVs on a residential distribution grid," *IEEE Trans. Power Syst.*, vol. 25, no. 1, pp. 371–380, Feb. 2010.
- [5] J. A. P. Lopes, F. J. Soares, and P. M. R. Almeida, "Integration of Electric Vehicles in the Electric Power System," *Proc. IEEE*, vol. 99, no. 1, pp. 168–183, Jan. 2011.
- [6] D. Divan and P. Kandula, "Distributed power electronics: An enabler for the future grid," *CPSS Trans. Power Electron. Appl.*, vol. 1, no. 1, pp. 57–65, Dec. 2016.
- [7] M. Kleinberg *et al.*, "Energy storage valuation under different storage forms and functions in transmission and distribution applications," *Proc. IEEE*, vol. 102, no. 7, pp. 1073–1083, Jul. 2014.
- [8] R. D. Masiello, B. Roberts, and T. Sloan, "Business models for deploying and operating energy storage and risk mitigation aspects," *Proc. IEEE*, vol. 102, no. 7, pp. 1052–1064, Jul. 2014.
- [9] A. Nagarajan and R. Ayyanar, "Design and strategy for the deployment of energy storage systems in a distribution feeder with penetration of renewable resources," *IEEE Trans. Sustain. Energy*, vol. 6, no. 3, pp. 1085–1092, Jul. 2015.
- [10] L. F. Costa, G. D. Carne, G. Buticchi, and M. Liserre, "The Smart Transformer: A solid-state transformer tailored to provide ancillary services to the distribution grid," *IEEE Power Electron. Mag.*, vol. 4, no. 2, pp. 56–67, Jun. 2017.
- [11] X. She, A. Q. Huang, and R. Burgos, "Review of solid-state transformer technologies and their application in power distribution systems," *IEEE J. Emerg. Sel. Topics Power Electron.*, vol. 1, no. 3, pp. 186–198, Sept. 2013.
- [12] P. Czyn, T. Guillod, F. Krismer, J. Huber, and J. W. Kolar, "Design and Experimental Analysis of 166 kW Medium-Voltage Medium-Frequency Air-Core Transformer for 1:1-DCX Applications," *IEEE J. Emerg. Sel. Topics Power Electron.*, 2021.
- [13] R. Zhu, M. Andresen, M. Langwasser, M. Liserre, J. P. Lopes, C. Moreira, J. Rodrigues, and M. Couto, "Smart transformer/large flexible transformer," *CES Trans. Elec. Mach. Syst.*, vol. 4, no. 4, pp. 264–274, Dec. 2020.
- [14] L. Zheng, R. P. Kandula, and D. Divan, "Soft-Switching Solid-State Transformer With Reduced Conduction Loss," *IEEE Trans. Power Electron.*, vol. 36, no. 5, pp. 5236–5249, May 2021.
- [15] A. Q. Huang, Q. Zhu, L. Wang, and L. Zhang, "15 kV SiC MOSFET: An enabling technology for medium voltage solid state transformers," *CPSS Trans. Power Electron. Appl.*, vol. 2, no. 2, pp. 118–130, 2017.
- [16] X. Han, L. Zheng, R. P. Kandula, K. Kandasamy, D. Divan, and M. Saedifard, "Characterization of 3.3 kV Reverse-Blocking SiC Modules for Use in Current-Source Zero-Voltage-Switching Converters," *IEEE Trans. Power Electron.*, vol. 36, no. 1, pp. 876–887, Jan. 2021.
- [17] C. Xu, J. Wei, L. Zheng, X. Han, M. Saedifard, R. P. Kandula, K. Kandasamy, D. Divan, and L. Graber, "Insulation Coordination Design for Grid-Connected Solid-State Transformers," *IEEE J. Emerg. Sel. Topics Power Electron.*, 2021.
- [18] U. Mehrotra, B. Ballard, and D. C. Hopkins, "Bidirectional Solid-State Circuit Breaker using Super Cascade for MV SST and Energy Storage Systems," *IEEE J. Emerg. Sel. Topics Power Electron.*, 2021.
- [19] T. Guillod, F. Krismer, and J. W. Kolar, "Protection of MV converters in the grid: The case of MV/LV solid-state transformers," *IEEE J. Emerg. Sel. Topics Power Electron.*, vol. 5, no. 1, pp. 393–408, Mar. 2017.
- [20] L. Zheng, X. Han, R. P. Kandula, K. Kandasamy, M. Saedifard, and D. Divan, "7.2 kV Three-Port Single-Phase Single-Stage Modular Soft-Switching Solid-State Transformer with Active Power Decoupling and Reduced DC-Link," in *Proc. IEEE Appl. Power Electron. Conf. Expo.*, 2020, pp. 1575–1581.

- [21] L. Zheng, X. Han, Z. An, R. P. Kandula, K. Kandasamy, M. Saedifard, and D. Divan, "SiC-Based 5 kV Universal Modular Soft-Switching Solid-State Transformer (M-S4T) for Medium-Voltage DC Microgrids and Distribution Grids," *IEEE Trans. Power Electron.*, vol. 36, no. 10, pp. 11326-11343, Oct. 2021.
- [22] D. Rothmund, T. Guillod, D. Bortis, and J. W. Kolar, "99% efficient 10 kV SiC-based 7 kV/400 V DC-transformer for future data centers," *IEEE J. Emerg. Sel. Topics Power Electron.*, vol. 7, no. 2, pp. 753-767, Jun. 2019.
- [23] W. Xu, Z. Guo, A. Vetrivelan, R. Yu, and A. Q. Huang, "Hardware Design of a 13.8kV/3MVA PV Plus Storage Solid State Transformer (PVS-SST)," *IEEE J. Emerg. Sel. Topics Power Electron.*, 2021.
- [24] A. Anurag, S. Acharya, S. Bhattacharya, T. R. Weatherford, and A. Parker, "A Gen-3 10 kV SiC MOSFETs based Medium Voltage Three-Phase Dual Active Bridge Converter Enabling a Mobile Utility Support Equipment Solid State Transformer (MUSE-SST)," *IEEE J. Emerg. Sel. Topics Power Electron.*, 2021.
- [25] Y. Sun, Z. Gao, C. Fu, C. Wu, and Z. Chen, "A Hybrid Modular DC Solid-State Transformer Combining High Efficiency and Control Flexibility," *IEEE Trans. Power Electron.*, vol. 35, no. 4, pp. 3434-3449, Apr. 2020.
- [26] J. Saha, N. B. Y. Gorla, A. Subramaniam, and S. K. Panda, "Analysis of Modulation and Optimal Design Methodology for Half-Bridge Matrix-Based Dual-Active-Bridge (MB-DAB) AC-DC Converter," *IEEE J. Emerg. Sel. Topics Power Electron.*, 2021.
- [27] R. Baranwal, K. V. Iyer, K. Basu, G. F. Castelino, and N. Mohan, "A Reduced Switch Count Single-Stage Three-Phase Bidirectional Rectifier With High-Frequency Isolation," *IEEE Trans. Power Electron.*, vol. 33, no. 11, pp. 9520-9541, Nov. 2018.
- [28] L. Zheng, R. P. Kandula, K. Kandasamy, and D. Divan, "Stacked Low-Inertia Converter or Solid-State Transformer: Modeling and Model Predictive Priority-Shifting Control for Voltage Balance," *IEEE Trans. Power Electron.*, vol. 36, no. 8, pp. 8934-8952, Aug. 2021.
- [29] L. Zheng, R. P. Kandula, and D. Divan, "Robust Predictive Control for Modular Solid-State Transformer with Reduced DC Link and Parameter Mismatch," *IEEE Trans. Power Electron.*, vol. 36, no. 12, pp. 14295-14311, Dec. 2021.
- [30] J. Chen, R. Zhu, I. Ibrahim, T. O'Donnell, and M. Liserre, "Neutral current optimization control for smart transformer-fed distribution system under unbalanced loads," *IEEE J. Emerg. Sel. Topics Power Electron.*, vol. 9, no. 2, pp. 1696-1707, Apr. 2021.
- [31] S. Bhawal, S. S. Chakraborty, and K. Hatua, "Dynamic Modeling and Closed Loop Control of a Solid State Transformer (SST) based on Series Resonant Converter (SRC)," *IEEE J. Emerg. Sel. Topics Power Electron.*, 2021.
- [32] S. Ouyang, J. Liu, X. Chen, and Y. Yang, "Control strategy for single-phase open-circuit operation of a modular solid-state transformer," *IEEE Trans. Power Electron.*, vol. 34, no. 9, pp. 8555-8573, Sep. 2019.
- [33] L. Zheng, R. P. Kandula, K. Kandasamy, and D. Divan, "New Modulation and Impact of Transformer Leakage Inductance on Current-Source Solid-State Transformer," *IEEE Trans. Power Electron.*, vol. 37, no. 1, Jan. 2021.
- [34] D. Dong, R. Raju, G. Ganireddy, and M. Agamy, "A Rotational Control in Medium-Voltage Modular Solid-State Transformer-Based Converter System," *IEEE Trans. Ind. Appl.*, vol. 55, no. 6, pp. 6223-6233, Nov.-Dec. 2019.
- [35] T. Isobe, R. A. Barrera-Cardenas, Z. He, Y. Zou, K. Terazono, and H. Tadano, "Control of Three-Phase Solid-State Transformer With Phase-Separated Configuration for Minimized Energy Storage Capacitors," *IEEE J. Emerg. Sel. Topics Power Electron.*, vol. 8, no. 3, pp. 3014-3028, Sept. 2020.
- [36] S. Essakiappan, H. S. Krishnamoorthy, P. Enjeti, R. S. Balog, and S. Ahmed, "Multilevel Medium-Frequency Link Inverter for Utility Scale Photovoltaic Integration," *IEEE Trans. Power Electron.*, vol. 30, no. 7, pp. 3674-3684, Jul. 2015.
- [37] J. Nie, L. Yuan, W. Wen, R. Duan, B. Shi, and Z. Zhao, "Communication-Independent Power Balance Control for Solid State Transformer Interfaced Multiple Power Conversion Systems," *IEEE Trans. Power Electron.*, vol. 35, no. 4, pp. 4256-4271, Apr. 2020.
- [38] C. Kumar, R. Zhu, G. Buticchi, and M. Liserre, "Sizing and SOC management of a smart-transformer-based energy storage system," *IEEE Trans. Ind. Electron.*, vol. 65, no. 8, pp. 6709-6718, Aug. 2018.
- [39] T. Zhao, X. Zhang, M. Wang, W. Mao, F. Li, F. Wang, and X. Wang, "Module Power Balance Control and Redundancy Design Analysis of Cascaded PV Solid-State Transformer Under Fault Conditions," *IEEE J. Emerg. Sel. Topics Power Electron.*, vol. 9, no. 1, pp. 677-688, Feb. 2021.
- [40] L. Zheng, R. P. Kandula, and D. Divan, "Current-Source Solid-State DC Transformer Integrating LVDC Microgrid, Energy Storage and Renewable Energy into MVDC Grid," *IEEE Trans. Power Electron.*, vol. 37, no. 1, Apr. 2021.
- [41] D. Atkar, P. Chaturvedi, H. M. Suryawanshi, P. Nachankar, and D. Yadeo, "Optimal Design of Solid State Transformer based Interlink Converter for Hybrid AC/DC Micro-Grid Applications," *IEEE J. Emerg. Sel. Topics Power Electron.*, 2021.
- [42] J. Liu, S. Zhong, J. Zhang, Y. Ai, N. Zhao, and J. Yang, "Auxiliary Power Supply for Medium-/High-Voltage and High-Power Solid-State Transformers," *IEEE Trans. Power Electron.*, vol. 35, no. 5, pp. 4791-4803, May 2020.
- [43] C. Zhao *et al.*, "Power electronic traction transformer—Medium voltage prototype," *IEEE Trans. Ind. Electron.*, vol. 61, no. 7, pp. 3257-3268, Jul. 2014.
- [44] X. Gao, F. Sossan, K. Christakou, M. Paolone, and M. Liserre, "Concurrent voltage control and dispatch of active distribution networks by means of smart transformer and storage," *IEEE Trans. Ind. Electron.*, vol. 65, no. 8, pp. 6657-6666, Aug. 2018.
- [45] X. She, A. Q. Huang, S. Lukic, and M. E. Baran, "On integration of solid-state transformer with zonal dc microgrid," *IEEE Trans. Smart Grid*, vol. 3, no. 2, pp. 975-985, Jun. 2012.
- [46] Z. Zou, G. D. Carne, G. Buticchi, and M. Liserre, "Smart transformer-fed variable frequency distribution grid," *IEEE Trans. Ind. Electron.*, vol. 65, no. 1, pp. 749-759, Jan. 2018.
- [47] Q. Ye, R. Mo, and H. Li, "Impedance Modeling and DC Bus Voltage Stability Assessment of a Solid-State-Transformer-Enabled Hybrid AC-DC Grid Considering Bidirectional Power Flow," *IEEE Trans. Ind. Electron.*, vol. 67, no. 8, pp. 6531-6540, Aug. 2020.
- [48] C. Gao, M. Feng, J. Ding, H. Zhang, J. Xu, C. Zhao, Z. Li, and G. Li, "Accelerated Electromagnetic Transient (EMT) Equivalent Model of Solid-State Transformer," *IEEE J. Emerg. Sel. Topics Power Electron.*, 2021.
- [49] J. Chen, M. Liu, T. O'Donnell, and F. Milano, "Modelling of Smart Transformers for Power System Transient Stability Analysis," *IEEE J. Emerg. Sel. Topics Power Electron.*, 2021.
- [50] J. Burkard and J. Biela, "Hybrid transformers for power quality enhancements in distribution grids - comparison to alternative concepts," in *Proc. NEIS Conf. Sustain. Energy Sup. and Energy Storage Syst.*, 2018, pp. 1-6.
- [51] J. Burkard and J. Biela, "Design of a protection concept for a 100-kVA hybrid transformer," *IEEE Trans. Power Electron.*, vol. 35, no. 4, pp. 3543-3557, Apr. 2020.
- [52] J. Burkard and J. Biela, "Evaluation of topologies and optimal design of a hybrid distribution transformer," in *Proc. IEEE Energy Convers. Congr. Expo. Europe*, 2015, pp. 1-10.
- [53] J. Kaniewski, Z. Fedyczak, and G. Benysek, "AC voltage sag/swell compensator based on three phase hybrid transformer with buck-boost matrix-reactance chopper," *IEEE Trans. Ind. Electron.*, vol. 61, pp. 3835-3846, Aug. 2014.
- [54] P. Szczesniak and J. Kaniewski, "Hybrid transformer with matrix converter," *IEEE Trans. Power Del.*, vol. 31, no. 3, pp. 1388-1396, Jun. 2016.
- [55] R. P. Kandula, A. Iyer, R. Moghe, J. E. Hernandez, and D. Divan, "Power router for meshed systems based on a fractionally rated back-to-back converter," *IEEE Trans. Power Electron.*, vol. 29, no. 10, pp. 5172-5180, Oct. 2014.
- [56] D. Das, D. M. Divan, and R. G. Harley, "Power flow control in networks using controllable network transformers," *IEEE Trans. Power Electron.*, vol. 25, no. 7, pp. 1753-1760, Jul. 2010.

- [57] D. Das, R. P. Kandula, J. A. Muñoz, D. Divan, R. G. Harley, and J. E. Schatz, "An integrated controllable network transformer—Hybrid active filter system," *IEEE Trans. Ind. Appl.*, vol. 51, no. 2, pp. 1692–1701, Mar./Apr. 2015.
- [58] R. P. Kandula, H. Chen, A. Prasai, F. Lambert, T. Heidel, C. Schauder, J. Schatz, T. Powell, and D. Divan, "Field test results for a 3-phase 12.47 kV 1 MVA power router," in *Proc. IEEE Energy Convers. Congr. Expo.*, 2016, pp. 1-8.
- [59] J. E. Huber and J. W. Kolar, "Applicability of solid-state transformers in today's and future distribution grids," *IEEE Trans. Smart Grid*, vol. 10, no. 1, pp. 317-326, Jan. 2019.
- [60] D. Divan and H. Johal, "Distributed FACTS—A new concept for realizing grid power flow control," *IEEE Trans. Power Electron.*, vol. 22, no. 6, pp. 2253-2260, Nov. 2007.
- [61] J. M. Bloemink and T. C. Green, "Benefits of distribution-level power electronics for supporting distributed generation growth," *IEEE Trans. Power Del.*, vol. 28, no. 2, pp. 911-919, Apr. 2013.
- [62] W. H. Kersting, "Radial distribution test feeders," in *Proc. IEEE Power Eng. Soc. Winter Meeting*, 2001, pp. 908-912.
- [63] S. Papathanassiou, N. Hatzargyriou, and K. Strunz, "A benchmark low voltage microgrid network," in *Proc. CIGRE Symp.*, 2005, pp. 1-8.
- [64] R. Middlebrook and S. Cuk, "A general unified approach to modeling switching-converter power stages," in *Proc. IEEE Power Electron. Specialists Conf.*, 1976, pp. 18–34.
- [65] C. Eid, J. R. Guillen, P. F. Marin, and R. Hakvoort, "The economic effect of electricity net-metering with solar PV: Consequences for network cost recovery, cross subsidies and policy objectives," *Energy Policy*, vol. 75, pp. 244–254, 2014.
- [66] M. Koller, T. Borsche, A. Ulbig, and G. Andersson, "Defining a degradation cost function for optimal control of a battery energy storage system," in *Proc. Power Tech*, 2013, pp. 1-6.
- [67] S. Boyd and L. Vandenberghe, "Convex optimization," *Cambridge Univ. Press*, 2004.
- [68] K. Ashok, M. J. Reno, and D. Divan, "Secondary network parameter estimation for distribution transformers," in *Proc. IEEE Innovative Smart Grid Tech. Conf.*, 2020, pp. 1-5.
- [69] R. P. Kandula, H. Chen, A. Prasai, F. Lambert, J. Schatz, and D. Divan, "Field upgradeable transformer: A fractionally-rated voltage regulator for the distribution system," in *Proc. IEEE Energy Convers. Congr. Expo.*, 2016, pp. 1-8.
- [70] D. Divan and J. Sastry, "Voltage synthesis using dual virtual quadrature sources—A new concept in AC power conversion," *IEEE Trans. Power Electron.*, vol. 23, no. 6, pp. 3004–3013, Nov. 2008.
- [71] Y. Zhang, "Solar Power Data for Integration Studies", NREL.gov. [Online]. Available: <https://www.nrel.gov/grid/solar-power-data.html#panel1>.
- [72] "Commercial and Residential Hourly Load Profiles for all TMY3 Locations in the United States", OpenEI.org. [Online]. Available: <https://openei.org/doe-opendata/dataset/commercial-and-residential-hourly-load-profiles-for-all-tmy3-locations-in-the-united-states>.
- [73] F. Ran, T. Remo, and R. Margolis, "U.S. Utility-Scale Photovoltaics-Plus-Energy Storage System Costs Benchmark," NREL, Golden, CO, USA. Tech. Rep. NREL/TP-6A20-71714. 2018.
- [74] F. M. Camilo, R. Castro, M. E. Almeida, and V. F. Pires, "Assessment of overvoltage mitigation techniques in low-voltage distribution networks with high penetration of photovoltaic microgeneration," *IET Renewable Power Gener.*, vol. 12, no. 6, pp. 649–656, 2018.
- [75] M. C. Cerbantes, R. F.-Blanco, M. A. O.-Vazquez, and J. R. S. Mantovani, "Incorporating a nodal reactive power pricing scheme into the disco's short-term operation," *IEEE Trans. Smart Grid*, vol. 10, no. 4, pp. 3720–3731, Jul. 2019.
- [76] C. de M. Affonso and M. Kezunovic, "Technical and economic impact of PV-BESS charging station on transformer life: A case study," *IEEE Trans. Smart Grid*, vol. 10, no. 4, pp. 4683–4692, Jul. 2018.
- [77] M. Koller, T. Borsche, A. Ulbig, and G. Andersson, "Review of grid applications with the Zurich 1 MW battery energy storage system," *Elec. Power Syst. Res.*, vol. 120, pp. 128–135, Mar. 2015.
- [78] F. Ran, T. Remo, and R. Margolis, "U.S. Solar Photovoltaic System Cost Benchmark: Q1 2018," NREL, Golden, CO, USA. Tech. Rep. NREL/TP-6A20-72399. 2018.



Liran Zheng (Member, IEEE) received the B.S. degree in control engineering from Tsinghua University, Beijing, China, in 2016, and the M.S. degree in electrical and computer engineering from Georgia Institute of Technology, Atlanta, GA, USA, in 2018, where he is currently working towards the Ph.D. degree with the Center for Distributed Energy.

He was a Visiting Student with the Center for Power Electronics Systems, Virginia Polytechnic Institute and State University, Blacksburg, VA, USA, and The University of Texas at Austin, Austin, TX, USA, in summer 2015 and fall 2014, respectively. He was a technical fellow intern with the General Electric Global Research Center, Niskayuna, NY, USA, in summer 2021. His research interests include power electronics and distributed energy resources.

Mr. Zheng was the recipient of a prize paper award from the IEEE Industry Application Society.



Aniruddh Marellapudi received the B.S. degree in biomedical engineering from Duke University, Durham, NC in 2017, and the M.S. degree in electrical engineering from the Georgia Institute of Technology, Atlanta, GA in 2020, where he is currently pursuing the Ph.D. with the Center for Distributed Energy.

In the summer of 2019, he worked with the Duke Electric Vehicles team to set the Guinness World Record for "Most Efficient Prototype Electric Vehicle" with an efficiency of 797 mi/kWh (27.482 MPGe). Also in the summer of 2019, he was an intern at Wolfspeed, Durham, NC, where he studied the impacts of nano-henry inductances in SiC MOSFET switching characterization testbeds. He is currently a Power Electronics Engineer with Endeavour Inspired Infrastructure, where he is designing the GridBlock, a plug-and-play, 500 kW multi-port energy router. His research interests include grid connected power electronics, renewable energy integration, and understanding optimal pathways to achieving 100% energy sustainability.



Vikram Roy Chowdhury received the B.Tech. degree from WBUT, Kolkata, India, in 2010 and the M.Tech. degree from the Indian Institute of Technology, Kharagpur, Kharagpur, India, in 2013, both in Electrical Engineering. He completed his Ph.D. degree in Electrical and Computer Engineering from Missouri University of Science and Technology, Rolla, MO, USA in September 2019 with a focus on smart control architecture for grid connected converters. He was a Post-doctoral research associate with the Electrical and Computer Engineering department at Georgia Institute of Technology, Atlanta, USA from Oct 2019 to Nov 2021. Currently he is a Post-doctoral research associate with National Renewable Energy Laboratory, at Golden Colorado, USA. His research interests include application of nonlinear control architecture for power electronics-based grid-connected/isolated renewable energy systems and electric drives.



Nishant Bilakanti (Student Member, IEEE) received the B.Tech. degree in electrical and electronics engineering from Vellore Institute of Technology, Vellore, India, in 2015. He is currently pursuing a Ph.D. degree in electrical and computer engineering at Georgia Institute of Technology, Atlanta, GA, USA. In 2019, he interned with the Autonomous Systems and Control group at Siemens Corporate Technology, Princeton, NJ, USA, and worked on the decentralized control of inverters and microgrids. In 2020, he interned with the Smart Grid and Emerging Technology group at ComEd, IL, USA, and worked on a distributed energy resource management system. His research interests include the grid integration and control of inverter-based distributed energy resources and microgrids.



Rajendra Prasad Kandula (Member, IEEE) received the B.E degree in electrical engineering from NIT, Nagpur, India in 2002, the M.E degree from IISC, Bangalore, India in 2004, and the Ph.D. degree in electrical engineering from Georgia Institute of Technology, Atlanta, GA, USA in 2014. He worked for three years in, Bharat Heavy Electricals Limited (BHEL) R&D, Hyderabad, as Design Engineer in the area of industrial drives and PV applications. He worked at Varentec, Santa Clara, as a Principal Engineer, mainly working in the area of development of power flow controllers and hybrid transformers for meshed transmission systems. He is currently working as a Chief Engineer with Center for Distributed Energy, Georgia Tech, Atlanta, USA. His main research interests include applications of power electronics for utility applications such as hybrid transformers, solid state transformers, hybrid filters, grid-forming converters, etc.



Maryam Saeedifard (Fellow, IEEE) received the Ph.D. degree in electrical engineering from the University of Toronto, Toronto, Canada, in 2008. She is currently as associate professor in the School of Electrical and Computer Engineering at Georgia Institute of Technology, Atlanta, GA, USA. Prior joining Georgia Tech, she was an Assistant Professor in the School of Electrical and Computer Engineering at Purdue University, West Lafayette, IN, USA. Her research interests include power electronics and applications of power electronics in power systems.



Santiago Grijalva (Senior Member, IEEE) received the Ph.D. degree in Electrical and Computer Engineering from the University of Illinois at Urbana-Champaign, Champaign, USA. He is the Southern Company Distinguished Professor of Electrical and Computer Engineering and Director of the Advanced Computational Electricity Systems (ACES) Laboratory at Georgia Institute of Technology, Atlanta, USA. From 2002 to 2009, he was with PowerWorld Corporation, Champaign, USA. From 2013 to 2014, he was with the National Renewable Energy Laboratory (NREL), Golden, USA as the Founding Director of the Power System Engineering Center (PSEC). He was a Member of the NIST Federal Smart Grid Advisory Committee. His research interests include decentralized power system control, cyber-physical security, and economics.



Deepak Divan (S'78–M'78–SM'91–F'98–LF'20) received the B.Tech. degree from Indian Institute of Technology, Kanpur, Kanpur, India, in 1975, and the M.Sc. and Ph.D. degrees from the University of Calgary, Calgary, AB, Canada, in 1979 and 1983, respectively, all in electrical engineering. He is currently John E. Pippin Chair Professor, GRA Eminent Scholar, and the Director of the Center for Distributed Energy, Georgia Institute of Technology, Atlanta, GA, USA. He works closely with utilities, industry, and is actively involved in research, teaching, entrepreneurship, and starting new ventures. He has started several companies, including Varentec, Santa Clara, CA, USA, where he served as a Founder, the President, and the CTO from 2011 to 2014, and as a Chief Scientist for several years after. He led the company as it developed its suite of innovative distributed real-time grid control technologies. Varentec was funded by leading green-tech Venture Capital firm Khosla Ventures and renowned investor Bill Gates. He has founded or seeded several new ventures, including Soft-Switching Technologies, Innovolt, Varentec, and Smart Wires, which together have raised >\$160 M in venture funding. He has 40 years of academic and industrial experience, 75 issued and pending patents, and over 400 reviewed publications. His field of research is in the areas of power electronics, power systems, smart grids, and distributed control of power systems. Dr. Divan is an Elected Member of the U.S. National Academy of Engineering, the National Academies Board on Energy and Environmental Systems, and the NASEM Committee on the Future Grid. He was a past President of the IEEE Power Electronics Society. He was a recipient of the IEEE William E Newell Field Medal and International Steering Committee Chair of the IEEE Empower a Billion Lives global competition to crowdsource scalable energy access solutions.